Eccentricity Fault Diagnosis Studying for a Round Rotor Synchronous Machine

PeymanNaderi[1], Sahar. M. Sharouni [2]

[1] Faculty of Electrical Engineering, ShahidRajaee Teacher Training University, Tehran, Iran,*Email: p.naderi@srttu.edu*
[2]Faculty of Electrical Engineering, Islamic Azad University of Borujerd , Borujerd, Iran,Email: Sahar.sharooni@yahoo.com

Abstract

The paper presents a mathematical base modeling combined to Modified-Winding -Function-Approach (MWFA) for eccentricity fault detection of a round-rotor synchronous machine. For this aim, a 6-pole machine is considered, and the machine inductances are computed by MWFA in healthy and also under eccentricity fault. A numerical discrete-time method has been proposed to machine modeling in voltage-fed case, and an exact analytical method is proposed to calculate the machine's currents and torque. A method is introduced for both static and dynamic eccentricity fault diagnosis, which is proposed for first time. A mathematical base method is introduced for machine modeling, and new results are obtained to a novel method addressing for eccentricity fault diagnosis. The method is validated by Finite-Element-Method (FEM) so accuracy of the proposed method is proofed.

Keywords: Air-gap function, dynamic eccentricity, static eccentricity, synchronous machine.

1. Introduction

This research is focused on the torque ripple and current spectrum of round rotor synchronous machine which is one of the electrical machines with rotor excitation. Although DQ0 transformation is one of the common methods for machine's analysis [1], it is not a proper choice for analyzing the machines with non-ideal properties such as slot opening effect or non-sinusoidal windings. In reality the machine normally has some torque ripples due to following reasons which are not considered in un-classical studies:

- Distributed winding which can produce a harmonically rotational field.
- Slot opening effect.
- Inexact air-gap function consideration.

On the other hand, eccentricity fault is one of the known faults that can occur in electrical machines. In the last decade, a number of researches have investigated this phenomenon and various papers have been published accordingly. In an old research, eccentricity fault has been considered by Joksimovic, et al. for a three-phase induction machine, however, the slot opening effect is missing in it [2]. In [3], eccentricity effect was studied on mutual inductance between rotor/stator arbitrary windings but a wide amount of summarizations have been assumed and torque/current signature was not addressed. In another work, eccentricity fault has been researched using current signature for silent pole synchronous and induction machines by Faiz, et al. via the electromagnetic equations and finite-element methods but did not proposed an exact model for air-gap function and machine's geometry [4-7]. The Current/Torque spectral analysis is the main approach for fault detection in electrical machines which were used for eccentricity and inter turn short circuit faults [4-12]. Wound rotor induction machine's faults were addressed in [8-12] by electromagnetic base modeling but the air-gap

function were roughly modeled and basic equations were employed for the modeling. It is known that the winding function theory (WFT) and Finite-Element-Method (FEM) are two powerful methods for numerical analysis of electrical machines. In [13], while slot opening and distributed winding effects are researched by Lubin, et al. for a synchronous reluctance machine's torque, the eccentricity fault and individual effect of each parameter is not addressed on machine parameters. The mathematical model in the research was introduced by WFT for a four-pole machine and the FEM analysis was considered for model validation. The same method has been used in [14], considering WFT, for a permanent magnet synchronous machine in which the magnets have been modeled by virtual coils. A 3-D FEM base eccentricity fault diagnosis for synchronous machine has been proposed by Iamamura, et al. in [15] wherein fault diagnosis has been confirmed using torque's signatures. The research performed only a series of simulation results without performing any dynamic model. In [16], a review is performed on induction machine fault diagnostic in the published paper in the recent decade by Bellini, et al. in which, various types of machine faults and diagnostic procedures were introduced. In [17], eccentricity faults in induction machines were studied based on terminal voltage at switch-off reveal certain future behavior. The paper presented a mathematical model but similarly to most of others, the slot opening effect was not considered. Since the condition monitoring is very useful for the machine maintenance, there are a number of general survey papers on this subject and the most relevant ones can be found in [18-20]. In addition to fault diagnosis, some researches have focused on healthy machines for torque/current spectral analysis which may have spectral components due to machine's mechanical structure. In [21], Stator-Current spectral signature was studied for healthy cage rotor induction machine and in [22], effect of slot-and-pole combination was addressed for performance analysis of Tooth-Coil synchronous machine by studying winding harmonic spectrum. However in both, the slot opening effect and behavior of faulty machine have not been considered. Therefore, other types of machines such as synchronous reluctance machines have been less investigated. Although in [23] WFT was used for dynamic eccentricity fault diagnosis in synchronous machine, validation of proposed method was not performed. In other work [24], the SynRM has been considered only for modeling and performance analysis by WFT but, modeling of slot openings and eccentricity fault analysis were not considered. As one can see, most of the above mentioned researches in fault diagnostic area have been carried out on induction and synchronous machines. So, there are a few papers which have focused on SynRM fault detection [25], [27]. As an existing research in this field was presented by Nandi, et al. in [25] but the research was performed by approximate electromagnetic equations such as the air-gap function and some damper bars have been considered on the rotor structure. Moreover, in [27] the eccentricity fault has been addressed by author for a sample SynRM. Now, this paper focus on the published paper by Ebrahimi et al. which addressed a method for dynamic eccentricity fault diagnosis in round rotor synchronous motor [26]. The authors had some mistakes in their assumptions for modeling and also signal processing to fault detection. Noticing that the synchronous machines has been less investigated for studying and eccentricity fault diagnosis, this research is focused on studying of mentioned behavior in healthy and faulty condition using a mathematical modeling with excellent accuracy and short simulation time consumption compared to FEM method which is normally used for validation in simulation part.

1. Case Study

In this research, performance analysis is considered to accurately compute the torque's ripple of a Three-Phase-Six-Pole round rotor synchronous machine (Fig. 1) with listed parameters in Table (1). The machine performance will compute in both healthy and faulty cases to a method presenting for dynamic eccentricity fault. According to the Fig. 1, stator has 72 slots and two-layer stator winding where four slots are assigned for each pole per phase per layer. Rotor has 30 slots were five slots have been assigned for each pole of field winding. As shown in Fig. 1, the reference of the stator circumambient ($\theta_s = 0$)and the reference of the rotor circumambient ($\theta_r = 0$) correspond with the center of winding (A) and the center of field winding (F) respectively. Considering the number of N_s turns for each pole per stator's phase, the number of $N_s/8$turns would exist in each slot per layer. Also, considering N_f turns for each pole of field winding, the number of$N_f/8$ turns would exist in each of rotor's slot. The machine's parameters and its structure have been shown in Fig.1. It should be noted that in order to use MWFA, there are some parts including air gap and winding functions that should be modelled for dynamic modelling.

A. Turn Functions

Sinusoidal winding function is an unreal property of a machine that cannot be assumed for realistic and excellent model because machines are not able to operate in their ideal status. In fact, limited number of slots is counted as one of the real factors that could lead to non-sinusoidal winding, turn and MMF functions. Noticing to slot numbers shown in Fig.1.c, the windings' map is listed in Table

(2). Regarding to mentioned map, Fig. 2 shows the turn function of phase 'A' and 'F' windings for relative sample machine, which has 8 and five slots per pole for stator and rotor respectively. Not to mention that, θ_s=0 and θ_r=0 implies that stator and rotor reference points are chosen at the center of 'A' and 'F' windings respectively. Two other winding functions of the stator can be obtained by 40 mechanical degrees shifting.

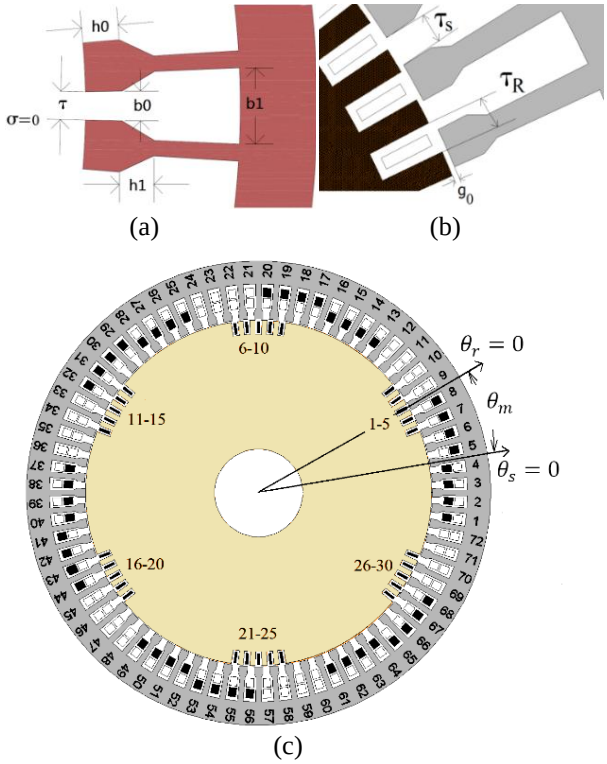

Fig. 1. The modelled machine structure. (a)- Geometric properties of slot (b)- Slot openings structure (c)- whole structure

Table.1.
The Modelled Machine Properties

Symbol	Parameter	Value
N_s	Stator phase's Turn per pole	160 turns
N_f	Rotor field's Turn	150 turns
R_f	Field winding resistance	1Ω
R_s	Stator winding resistance	2Ω
τ_s	Angle of stator slot opening	2.2°
τ_r	Angle of rotor slot opening	2.2°
γ_s	Stator slot pitch	5°
γ_r	Rotor slot pitch	4°
g_0	Constant part of air gap	0.5mm
r	Stator radius	7.5cm
l	Machine length	25cm
b0,b1	Slot's width properties	2.97,7.51mm
h0,h1	Slot's depth properties	3.71,3.51mm
N_{slot}	Number of slots	72
N_{Poles}	Number of poles	6

Table.1.
The Winding Map of Modelled Machine

	Stator winding map					
	$\uparrow A$	$\downarrow A$	$\uparrow A$	$\downarrow A$	$\uparrow A$	$\downarrow A$
Layer 1	1-4	13-16	25-28	37-40	49-52	61-64
Layer 2	5-8	17-20	29-32	41-44	53-56	65-68
	$\uparrow B$	$\downarrow B$	$\uparrow B$	$\downarrow B$	$\uparrow B$	$\downarrow B$
Layer 1	25-28	37-40	49-52	61-64	1-4	13-16
Layer 2	29-32	41-44	53-56	65-68	5-8	17-20
	$\uparrow C$	$\downarrow C$	$\uparrow C$	$\downarrow C$	$\uparrow C$	$\downarrow C$
Layer 1	49-52	61-64	1-4	13-16	25-28	37-40
Layer 2	53-56	65-68	5-8	17-20	29-32	41-44
	Field winding map					
	$\uparrow F$	$\downarrow F$	$\uparrow F$	$\downarrow F$	$\uparrow F$	$\downarrow F$
	1-5	6-10	11-15	16-20	21-25	26-30

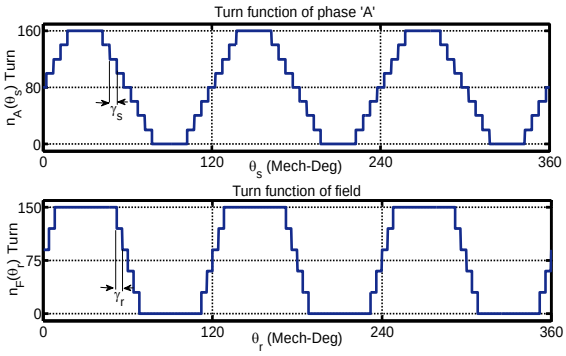

Turn functions of phase 'A' and field windings

Air-gap function in healthy and faulty cases

The air-gap function consists of three parts, which are stator's slot openings, rotor's slot openings and the gap length between the rotor and stator teeth. Slot opening geometry is another non-ideal property of a real machine. However, the proper function should be considered for slot opening to achieve the higher accuracy of the modelling. Relative figures are shown in Fig. 1.a and relevant mathematical model has been written in (1) for a half slot-gap that is proposed in [13], [27]-[29].

$$f_g(\sigma)= \begin{cases} \pi/2\, r\sigma & 0 \le r.\sigma \le h0 \\ \pi/2\, r\sigma + \vartheta(r.\sigma - h0) & h0 \le r.\sigma \le \tau/2 \end{cases} \quad (1)$$

Where,

$$\vartheta = \pi/2\, r\sigma - tan^{-1}(2h1/(b1 - b0)). \quad (2)$$

Now, the gap function for each slot can be computed as equation (3) [27]-[29].

$$s(\sigma) = f_g(\sigma) + f_g(-\sigma + \tau) \quad (3)$$

The gap function for stator's slots ($f_s(\theta_s)$) and also the gap function for rotor's slots ($f_r(\theta_r)$) can be modeled by (4) and (5) where, γ denotes the mechanical slot pitch as written in (6). It is notable that with regard to Fig. 4, equation (7) should be

considered due to the rotor position (θ_m) because the rotor position is particularly pertinent to stationery mechanical angle of stator and eccentricity coefficient (δ) [27], [28].

Eccentricity fault is caused because of ball bearing erosion and machine obsolescence and due to which, un-uniformed air gap will be produced.It has three cases named Static, Dynamic and Mixed eccentricity. As shown in Fig. 4, in static case, the rotor's rotation path is around the rotor center while in dynamic case, the rotation path is around the stator's center. Third condition is a combination of static and dynamic conditions as shown in Fig. 4.The conventional air-gap functions($f_t(\theta_s, \theta_m)$) under healthy and both dynamic and static eccentricity has been written in (8) and $\vartheta = 90^o$ denotes the center of fault at $\theta_r = -90^o$ and $\delta = 0$ denotes to healthy machine. Now, the whole air-gap function consists of all slots and rotor-stator conventional gap can be written as (9). Fig.5 shows the whole air-gap function in dynamic eccentricity for two sample rotor positions which has some effects due to machine slots and eccentricity fault.

$$f_s(\theta_s) = \sum_{k=0}^{72} s(\theta_s + \tau_s/2 + \gamma_s/2 - k.\gamma_s) \quad (4)$$

$$f_r(\theta_i) = \sum_{k=-90}^{90} s(\theta_r + \tau_r/2 - k.\gamma_r) \quad (5)$$

$$\gamma_i = 2\pi/n_i \quad \text{for i= 's' or 'r'} \quad (6)$$

$$\theta_r = \theta_s - \theta_m + tan^{-1}(\delta g_0/r).cos(\theta_s) \quad (7)$$

$$f_t(\theta_s, \theta_m) = g_0(1 + \delta.Cos(\theta - \vartheta)$$
$$\theta = \begin{cases} \theta_s & for\ Static\ Fault \\ \theta_r & for\ Dynamic\ Fault \end{cases} \quad (8)$$

$$f_g(\theta_s, \theta_m) = f_t(\theta_s, \theta_m) + f_s(\theta_s) + f_r(\theta_s, \theta_m) \quad (9)$$

2. Machine Inductances

Considering l_{li}as leakage inductance of ith winding, modified winding function theory (MWFT) [2], [3] has been used for calculating the machine's inductances as written in (10) using the turn functions shown in Fig 2. Moreover a constant inductance is used for natural of star connection. In case of $L_n \to \infty$ the float star connection can be modeled. According to (11) – (13) combined with equation (9), self and mutual inductances can be computed by the turn functions while air-gap function consists of three parts including rotor slots (f_r), stator slots (f_s) and conventional air-gap (f_t) as written in (10). It is a key not that the integral values in (11)-(13) should be computed in various $\theta_m$by a numerical method due to non-classic functions for integration. Using $\Delta\theta_m = 0.5^\circ$ the integration has been computed for 2π which mean to 721 time integration. The machine inductances and some of the computed inductances are shown in Fig.6. As shown in figure, the eccentricity fault has significant effect on the mutual field inductance due to eccentricity fault in term of oscillation frequency.

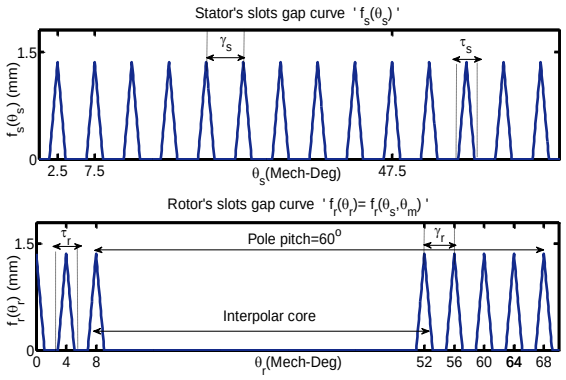

Fig. 2. Slot-gap functions of phase 'A' and field windings

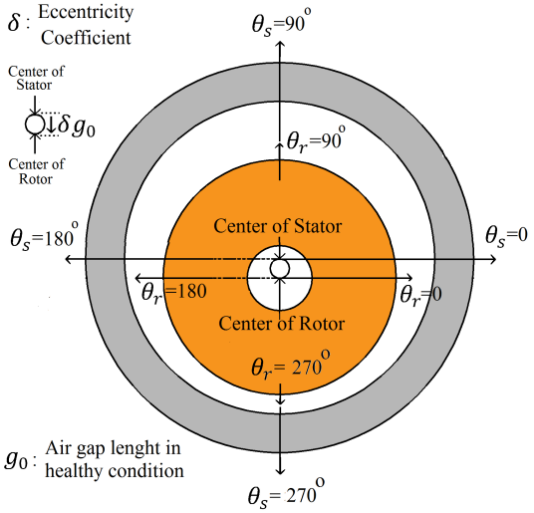

Fig. 3. Illustration of eccentricity fault, coefficients and relationship of mechanical angles

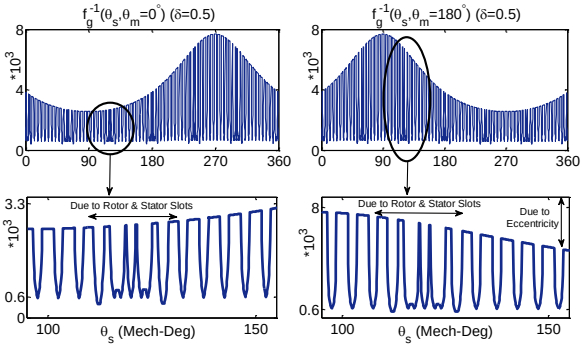

Fig. 4. The inverse of air-gap function in dynamic eccentricity with $\delta = 0.5$

Moreover some high frequency components are present due to slot numbering in both healthy and faulty cases.

$$L(\theta_m) = \begin{bmatrix} L_{AA}+L_{ls} & L_{AB} & L_{AC} & L_{AF} \\ L_{AB} & L_{BB}+L_{ls} & L_{BC} & L_{BF} \\ L_{AC} & L_{BC} & L_{CC}+L_{ls} & L_{CF} \\ L_{AF} & L_{BF} & L_{CF} & L_{FF}+L_{lF} \end{bmatrix} + \begin{bmatrix} L_n & L_n & L_n & 0 \\ L_n & L_n & L_n & 0 \\ L_n & L_n & L_n & 0 \\ 0 & 0 & 0 & 0 \end{bmatrix} \quad (10)$$

$$L_{ij}(\theta_m) = \mu_0 . l . r . [\int_0^{2\pi} n_i(\theta_s,\theta_m) . n_j(\theta_s,\theta_m) . f_g^{-1}(\theta_s, - 2\pi \langle M_i(\theta_s,\theta_m)\rangle . \langle M_j(\theta_s,\theta_m)\rangle . \langle f_g^{-1}(\theta_s,\theta_m) \quad (11)$$

$$\langle f_g^{-1}(\theta_s,\theta_m)\rangle = \frac{1}{2\pi}\int_0^{2\pi} f_g^{-1}(\theta_s,\theta_m) . d\theta_s \quad (12)$$

$$\langle M_k(\theta_s,\theta_m)\rangle = \frac{1}{2\pi\langle f_g^{-1}(\theta_s,\theta_m)\rangle}\int_0^{2\pi} n_k(\theta_s,\theta_m) . f_g^{-1}(\theta_s,\theta_m) d\theta_s \quad (13)$$

3. Dynamic Equations

Considering a three-phase voltage source as a power supply, the machine equation can be written as (14)-(16).

$$V = R . I + d\lambda/dt \quad (14)$$
$$\lambda = L . I \quad (15)$$
$$\tau_e = 1/2 . I^T . dL/d\theta_m . I \quad (16)$$

where,R is a diagonal matrix consist of winding's resistances and $I = [I_A \quad I_B \quad I_C \quad I_F]^T$, $V = [V_A \quad V_B \quad V_C \quad V_F]^T$, $\lambda = [\lambda_A \quad \lambda_B \quad \lambda_C \quad \lambda_F]^T$and The mechanical equation for speed calculation can be written as (17) for motoring operation. It is notable that the speed will be considered as a synchronous speed for generating operation.

$$\tau_e(t) - \tau_l(t) = j\frac{d\omega_m(t)}{dt} + B . \omega_m(t) \ , \quad \theta_m(t) = \omega_m(t) . t + \theta_m(0) \quad (17)$$

Considering (18) for discrete integration a numerical discrete method can be used for solving of equations (14)-(17) which can be written in (18)-(21).

$$\int_{t-\Delta t}^{t} f(t) = \Delta t/2 \left(f(t) + f(t-\Delta t)\right) \quad (18)$$

(19)

$$\lambda(t) = (I + \Delta t/2 . R . L(t)^{-1})^{-1} . [\Delta t/2 . V(t) + \Delta t/2 . V(t-\Delta t) + (I - \Delta t/2 . R . L(t-\Delta t)^{-1}) . \lambda(t - \Delta t)]$$

$$I(t) = L(t)^{-1} . \lambda(t) \quad (20)$$

(21)

$$\omega_m(t) = (1 + B . \Delta t/2j)^{-1} . [\Delta t/2j . \tau_e(t) + \Delta t/2j . \tau_e(t-\Delta t) - \Delta t/2j . \tau_l(t) - \Delta t/2j . \tau_l(t-\Delta t) - (B . \Delta t/2j - 1) . \omega_m(t-\Delta t)]$$

Where, $L(t) = L(\theta(t)/\omega(t))$ and the machine torque can be computed by (16) at each given time. It is notable that the rotational speed can be considered equal to synchronous speed for generating mode operation.

4. Eccentricity Fault Detection

In this part a numerical base method according to equations (19)-(21) and (16), has been confirmed to evaluate of machine behaviour in healthy and faulty cases. The eccentricity coefficient is considered equal to $\delta = 0.5$ float star connection has been considered by using $L_n \to \infty$ in the equation (10). The simulation has been performed in two cases as following:

– Generating operation with constant synchronous speed as (22).
– Motoring operation with constant load torque as (23).

In both cases a symmetrical 380 V-three-phase -60 Hz voltage source has been considered as the stator voltage source as written in (24). Moreover a 10 V voltage source is considered for field voltage. It is notable that $\theta_m(0)$ can be tuned for the output torque in generating mode.

$$\omega_m(t) = \omega_s/3, \ \omega_s = 2\pi \times 60 \quad (22)$$

$$\tau_l(t) = 5 \ N.m \quad (23)$$

$$V_A(t) = 220\sqrt{2} . \cos(2\pi \times 60t)$$
$$V_B(t) = 220\sqrt{2} . \cos(2\pi \times 60t - 2\pi/3) \quad (24)$$
$$V_C(t) = 220\sqrt{2} . \cos(2\pi \times 60t + 2\pi/3)$$

Some parts of results are shown in Fig.7 -10 for healthy and faulty machine. As shown in Fig. 7, there are minor effects in torque and stator currents waveform in faulty cases but there are more effect on the field current in both motoring and generating modes. Moreover the motor speed has some low frequency components in faulty cases. Regarding to results as shown in Figs.7 the machine torque and also the machine currents has not significant effect due to eccentricity fault so the power spectral density may be used for the fault detection.. It is notable that the field current has the mean value equal to 10 A in both motoring and generating modes.

Moreover, the machine speed has 1200 rpm as the mean value of rotor speed. Another notable fact is some high harmonically component which are present in the machine currents and the output torque and also the machine speed in motoring and generating modes that are produced due to slot openings, slot numberings and also non-sinusoidal

turn functions. Regarding to Figs. 7 there are not a visible signature in the both machine currents and the output torque in time domain. So, the power spectral density (PSD) should be used to obtaining of a method for eccentricity fault detection. Regarding to obtained results as shown in Figs 8 and 9, there are a certain produced components in both static and dynamic faults which have been tabulated in Table (3). The results shows in Figs 8 and 9 are obtained for the torque and current spectrum in three cases for both motoring and generating modes. Clearly the produced component in both static and dynamic eccentricity faults can be visible as tabulated components as listed in Table (3).

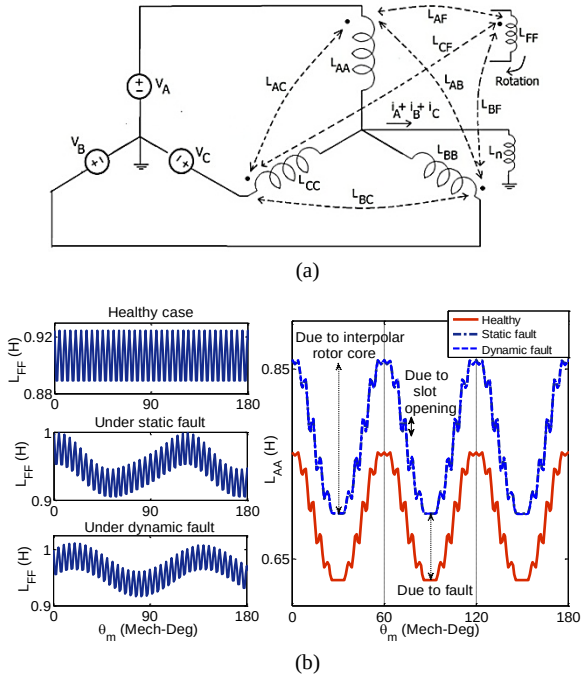

Fig. 5. (a)-Machine inductances and supplying structure (b) some of the computed inductances based on MWFA in healthy and faulty conditions with $\delta = 0.5$.

Table.2.
The Produced Component In Healthy and Faulty Machine

	Torque components	Current components
Healthy	$6\times kf_s$	$6\times (k\pm1)f_s$
Dynamic eccentricity	$k\times f_s/3$	$k\times f_s/3$
Static eccentricity	$k\times f_s$	$k\times f_s$

5. Comparison With FEM

In this part the machine operation has been simulated by Maxwell software which is based on the Finite-Element-Method (FEM) for comparison. The machine has been considered in generating mode and simulation has been performed in both healthy and faulty cases with static and dynamic eccentricity faults. The stator current spectrum is shows in Fig 10 and it is clear that the produced component in healthy and faulty cases has completely agreement with the proposed method as listed in Table (3). It is an important note that the FEM analysis has very longer time for simulation compare to proposed mathematical base method. So, the proposed method is very powerful for electrical machine studying such as fault detection analysis.

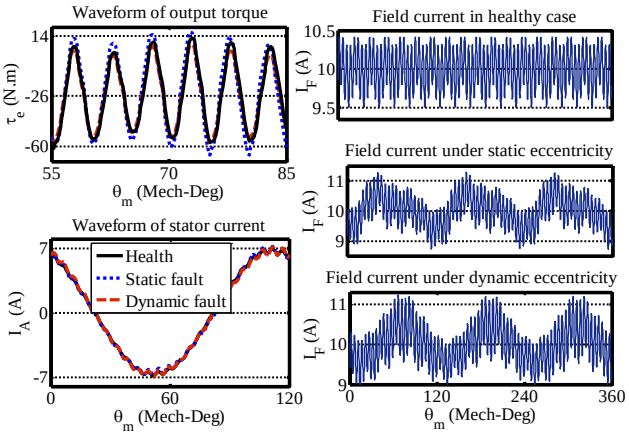

Fig. 6. Torque curve and machine currents in generating mode with $\theta_m(0) = 6^\circ$

6. Conclusion

In this paper, a mathematical base modeling was addressed for dynamic equation of an electrical machine modeling, and MWFA was used for inductance computation. The method used for modeling of a round-rotor-synchronous machine in healthy and faulty cases, and a new method was presented for both dynamic and static eccentricity fault detection, which was presented for first time. The validation made by Finite-Element-Method (FEM) shows an excellent result, which were obtained by the proposed method. The new results for eccentricity fault detection and also the mathematical base method for modelling of machine dynamic equations are the more advantages of paper.

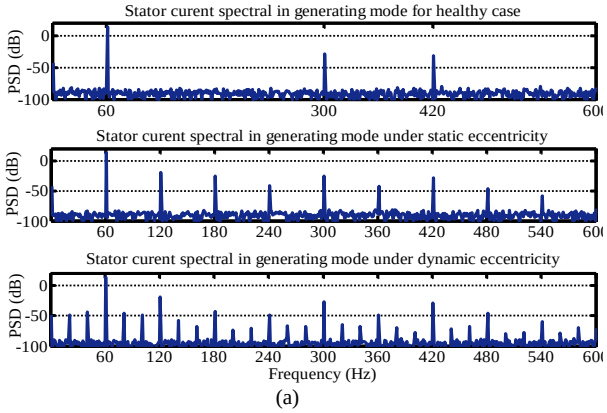

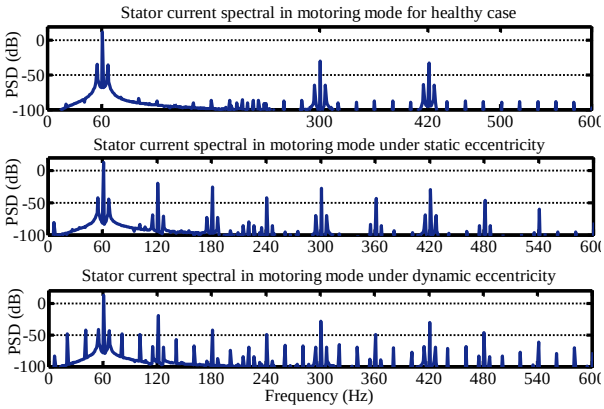

(b)

Fig. 7. PSD of stator currents in healthy and faulty cases. (a) in generating mode (Rotational speed has a constant value equal to synchronous speed) (b) in motoring mode with constant load torque.

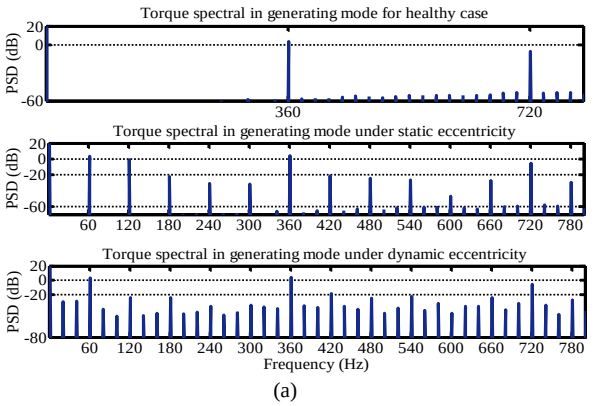

(a)

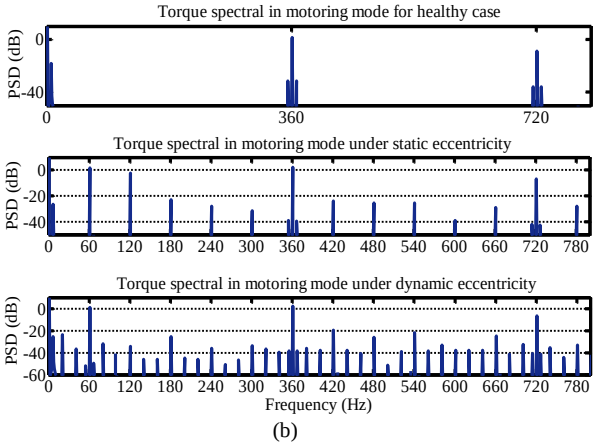

(b)

Fig. 8. PSD of output current in healthy and faulty cases. (a) in generating mode (Rotational speed has a constant value equal to synchronous speed) (b) in motoring mode with constant load torque.

References

[1] Electrical Machine Design, Third Chapter of book, Sawni. P.178-183.

[2] G. M. Joksimovic, D. J. Penman, and N. Arthur, "Dynamic Simulation of Dynamic Eccentricity in Induction Machine-Winding Function Theory", IEEE Transaction on Energy Conversion, Vol. 15, No.2, June 2000.

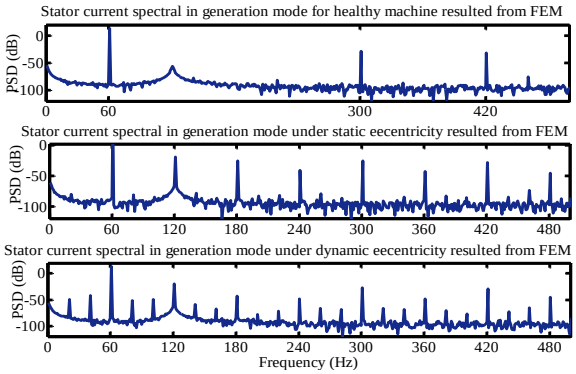

Fig. 9. Obtained results by FEM (a) stator current spectrum in healthy and faulty cases (b) torque and stator current

[3] J. Faiz, I. Tabatabaee, "Extension of Winding Function Theory for Non-uniform Air Gap in Electrical Machinery", IEEE Transaction on Magnetics, Vol.38, No.6, November 2002.

[4] [4] J. Faiz, B. M. Ebrahimi, B. Akin, and H.A. Toliyat, "Finite Element Transient Analysis of Induction Motors Under Mixed Eccentricity Fult", IEEE Transaction on Magnetics, Vol. 44, No.1, January 2008.

[5] B.M. Ebrahimi, J. Faiz, B.N. Araabi, "Pattern identification for eccentricity fault diagnosis in permanent magnet synchronous motors using stator current monitoring", IET Electric power Application, Vol.4, Issue.6, 2010.

[6] B.M. Ebrahimi, J. Faiz, " Magnetic field and vibration monitoring in permanent magnet synchronous motors under eccentricity fault", IET Electric Power Application, Vol.6, Issue.1, 2012.

[7] B. M. Ebrahimi, J. Faiz, "Diagnosis and performance analysis of three-phase permanent magnet synchronous motor with static, dynamic and mixed eccentricity", IET electric Power Application., Vol. 4, No.1, 2010.

[8] S. Djurovic, D.S. Vilchis-Rodriguez, A.C. Smith, "Vibration monitoring for wound rotor induction machine winding fault detection," Electrical Machines (ICEM), 2012 XXth International Conference on , vol., no., pp.1906,1912, 2-5 Sept. 2012.

[9] [9] Williamson, S.; Djurovic, S., "Origins of stator current spectra in DFIGs with winding faults and excitation asymmetries," Electric Machines and Drives Conference, 2009. IEMDC '09. IEEE, pp.563, 570, May 2009.

[10] S. Djurović, D.S. Vilchis-Rodriguez, A.C. Smith, 'Investigation of wound rotor induction machine vibration signal under stator electrical fault conditions', The IET Journal of Engineering, 2014.

[11] Larose. C, Gagnon. R. Prud'Homme/ P, Fecteau. M. Asmine. M., "Type-III Wind Power Plant Harmonic Emissions: Field Measurements and Aggregation Guidelines for Adequate Representation of Harmonics," Sustainable Energy, IEEE Transactions on Sustainable Energy , vol.4, no.3, pp.797,804, July 2013.

[12] Shah, D.; Nandi, S.; Neti, P., "Stator-Inter-turn-Fault Detection of Doubly Fed Induction Generators Using Rotor-Current and Search-Coil-Voltage Signature Analysis," IEEE Transactions on Industry Applications, vol.45, no.5, pp.1831,1842, Sept.-oct. 2009.

[13] T. Lubin, T. Hamiti, H. Razik, and A. Rezzoug, "Comparison Between Finite-Element Analysis and Winding Function Theory for Inductances and Torque Calculation of a Synchronous Reluctance Machine. IEEE Transaction on Magnetics, Vol. 43, No. 8, August 2007.

[14] S. Saied, K. Abbaszadeh, and A. Tenconi, "Improvement of

Winding Function Theory for PM Machine Analysis", International Conference on Power Engineering, Energy and Electrical Drives, Malaga, Spain, May 2011.

[15] B. A. T. Iamamura, Y. Le. Menach, A. Tounzi, N. Sadowski, E. Guillot, "Study of Static and Dynamic Eccentricities of a Synchronous Generator Using 3-D FEM," IEEE Transaction on Magnetic., Vol. 46, no.8,pp.3516-3519, August. 2010.

[16] A. Bellini, F. Filippeti, C. Tassoni, and G. A. Capolino, "Advances in Diagnostic Technique for Induction Machines", IEEE Transaction on Industrial Electronic, Vol. 55, No.12, Dec/2008.

[17] S. Nandi, T. Chelvan, S. B. Lee, and D. Hyun, "Detection of Eccentricity Faults in Induction Machine Base on Nameplate Parameters", IEEE Transaction on Industrial Electronic, Vol.58, No. 5, May/2011.

[18] M. Benbouzid, "A review of induction motors signature analysis as a medium for fault detection," IEEE Transaction on Industrial Electronic, vol.47, no.5, pp. 984-993, Oct.2000.

[19] S. Nandi, H. A. Toliyat, and X. Li, "Condition Monitoring and fault diagnosis of electrical motors-A review," IEEE Transaction on Energy Convers., vol. 20, no.4, pp 719-729, Dec. 2005.

[20] R. M. Tallam, S. B. Lee, G. C. Stone, G. B. Kliman, J. Yoo, T. G. Heabetler, and R. G. Harley, "A Survey of methods for detection of stator related faults in induction machines," IEEE Transaction on Industrial Electronic., vol. 43, no.4, pp. 920-933, Jun/Aug. 2007.

[21] G.M. Joksimovich, J.R. Thomson, M. Wolbank, Nedjeljko, and M. Vasak, "Stator-Current Spectrum Signature of Healthy Cage Rotor Induction Machines", IEEE Transaction on Industrial Electronics, Vol. 60, No. 9, September 2013.

[22] P. Ponomarev, P. Lindh, J. Pyrhonen, " Effect of Slot-Poles Combination on the Leakage Inductance and the Performance of Tooth-Coil Permanent-Magnet Synchronous Machines", IEEE Transaction on Industrial Electronics, Vol. 60, No. 10, October 2013.

[23] I. Tabatabaee, J. Faiz, H. Lessani, T.N. Razavi, "Modeling and Simulation of a Salient-Pole Synchronous Generator with Dynamic Eccentricity Using Modified Winding Function Theory", IEEE Transaction on Magnetic, Vol. 40, No. 3, May 2004.

[24] T. Hamity, T. Lubin, and A. Rezzoug, "A Simple and Effective Tool for Design Analysis of Synchronous Reluctance Motor", IEEE Transaction on Magnetic, Vol. 44, No. 12, December 2008.

[25] T.C. Ilamparithi, S. Nandi, "Detection of Eccentricity Faults in Three-Phase Reluctance Synchronous Motor", IEEE Transaction on Industry Application, Vol. 48, No. 4, July/August 2012.

[26] B.M. Ebrahimi, M. Etemadzadeh, J. Faiz, "Dynamic Eccentricity Fault Diagnosis in Round Rotor Synchronous Motors", Energy Conversion and Management,, pp. 2092-2097, 52, 2011.

[27] P. Naderi, "Eccentricity Fault Diagnosis and Torque Ripple Analysis of a Four-pole Synchronous Reluctance Machine in Healthy and Faulty Conditions", Electric power component and systems, Vol. 43, No.11, pp. 1236-1245, Jun. 2015.

[28] P. Naderi, A. Shiri, "Pole Arc Skewing Analysis of Synchronous Reluctance Machine Using Discrete Method Combined with Winding Function Approach,". The applied computational electromagnetic society, Vol.30, No.7, pp. 731-739, July. 2015.

[29] P. Naderi, A. Taheri, "Slot Numbering and Distributed Winding Effects Analysis on the Torque/Current Spectrum of Three-Phase-Wound-Rotor Induction Machine, using Discrete Modeling Method", Electric power component and systems, Vol. 43, No.15, pp. 1236-1245, August. 2015.

Coordinated Design of PSS and SSSC Damping Controller Considering Time Delays using Biogeography-based Optimization Algorithm

Javad Gholinezhad[1], Mahmoud Ebaadian[2], Mohammad R. Aghaerrahimi[3]

[1]*Faculty of Electrical and Computer Engineering,University of Birjand, Birjand, Iran, Email:Gholinezhad.javad@gmail.com*

Abstract

In this paper, a consistent pattern with the optimal coordinated design of PSS and SSSC controller to improve the damping of low frequency oscillations is shown. In this design, sensing and signal transmission time delays are considered as effectiveness parameters. The design problem has been considered an optimization problem and biogeography-based optimization (BBO) algorithm is used for searching the optimal controller parameters. The proposed controller is employed for a single machine and two-machine power systems. The results are displayed in different load conditions to present the efficiency of the proposed method. The proposed controller provides sufficient damping for power system oscillations, in different operating conditions and disturbances. Results analysis shows that the use of biogeography-based optimization algorithm has a higher efficiency in damping oscillations of the power system, compared with the PSO algorithm, and increases the dynamic stability more.

Keywords: Power System Stabilizer; Static Synchronous Series Compensator; Damping Controller; Dynamic Stability; BBO.

1. Introduction

When power systems expanded and connected together with weak tie lines, the low-frequency oscillations are increased and the stability margin of the power system decreases. If enough damping does not exist in power system, these oscillations remain and grow until the system breaks down [1]. Power System Stabilizers (PSSs) are usually used in power systems for damping oscillations [2]. However, due to the increased load on the transmission lines over long distances, using PSS alone is not providing enough damping and with PSS, other effective options are required. The rapid progress of power electronic devices has made the use of Flexible AC Transmission Systems (FACTS) possible in controlling power systems. FACTS controllers are able to quickly control network situation in different operating conditions and this ability of FACTS controllers can improve power system stability [3,4]. SSSC is a FACTS device connected in series with power transmission lines. SSSC can control power flow very effectively and can inject series inductive or capacitive voltage. The performance of SSSC in improving the stability and power oscillations damping can be seen in many references [5-7].

The coordinated design of SSSC controller and PSS may decrease or increase the damping in some oscillation modes. A lot of research on coordinated design of PSS and FACTS devices has been carried out [8]. When PSS is located near the generator and FACTS devices have been installed at a distance away from the generator, the sensing and signal transmission time delays should be considered in the design of FACTS controller and PSS. However, the influence of these time delays is not considered in the

previously published papers. One of the major issues which must be investigated in the coordinated design methods, is the ability and the robustness of the designed controller. Therefore, the efficiency and effectiveness of the controller in the power system operation should be considered.

In many papers, FACTS device damping controllers are proposed based on artificial intelligence [9-11]. In this paper, a complete evaluation of the efficacy and safety has been carried out in coordinated design of PSS and SSSC damping controller. The problem of robust coordinated design of PSS and SSSC-based damping controller is converted to an optimization problem. To adjust and optimize the controller parameters of SSSC and PSS, Biogeography-Based Optimization (BBO) algorithm is used. The proposed controller is used in single-machine and two-machine power systems. Simulation results under various operating conditions and disturbances show the efficiency and effectiveness of the proposed damping controller. In this study, all of the necessary dynamics of power system stability have been used. The general conclusions obtained and the proposed controller can be used for large actual power systems.

2. Biogeography-based Optimization Algorithm

Biogeography is the study of the geographical distribution of organisms. In this method, the mathematical equations governing the distribution of organisms have been used as a basis for optimization. Biogeography explains how different kinds migrate between places, how they are created and how they are extinct. In fact, it explores the cause of changes in the distribution of kinds in various surroundings. The surroundings of Biogeography-Based Optimization algorithm is as an archipelago and any possible answer to optimize the problem is a residence. Geographic areas are habitats for species that are introduced as habitat suitability index (HSI). The every specificity of solution is entitled a suitability index variable (SIV). Habitats with high HSI can optimize the problem effectively and habitats with low HSI have less impact on the optimization problem. Habitats that have high HSI tend to have a large number of species while habitats with low HSI have few species. New generation in BBO occurs by combining the answer features to immigrate to other islands, and the answer features to migrate from other islands. Mutation in BBO for all population is performed in a state similar to PSO algorithm [12-14].

If probability that habitat includes S species at time "t" is shown by , is as follows at time "$t+\Delta t$":

$$P_S(t+\Delta t) = P_S(t)(1-\lambda_S \Delta t - \mu_S \Delta t) + P_{S-1}\lambda_{S-1}\Delta t + P_{S+1}\mu_{S+1}\Delta t \quad (1)$$

Where μ_S and λ_S are the rates of emigration and immigration, when S kinds exist in the island or habitat as displayed in Figure 1. According to this equation, S kinds exist at time "$t+\Delta t$" in one of the following possibilities:

- S kinds at "t", and there were not emigration and immigration between periods t and "$t+\Delta t$".
- S-1 kinds at "t", and there was an immigrating kind.
- S+1 kinds at "t", and there was an emigrating kind.

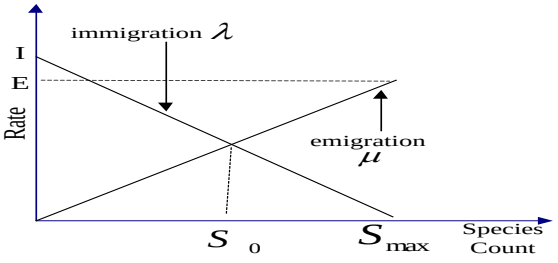

Fig. 1. Species model of a single habitat

According to figure 1, the equations giving the rates of immigration and emigration rates for the Kth species are as follows:

$$\mu_k = \frac{Ek}{n} \quad (1)$$

$$\lambda_k = I\left(1-\frac{k}{n}\right) \quad (2)$$

When $E = I$, the equations (3) and (4) are as follows:

$$\lambda_k + \mu_k = E \quad (3)$$

E and I are the initial emigration rate and the initial immigration rate, respectively. In BBO, as described, two basic operators exist, i.e. the migration and the mutation. Information is distributed between the existing solutions by migration operator. Especially, the weaker solutions get useful information from better solutions. The flowchart of Biogeography-Based Optimization algorithm is shown in Figure 2.

3. Power System Modelling

A. Generator model

Synchronous generators are one of the main components of any power system. Three sets of differential equations are required to represent the dynamic behavior of a synchronous generator. These sets of equations include the electrical equations (the field, damper bar and stator windings), mechanical equations (the rotor) and dynamic equations related to different control loops (such as AVR and turbine-

governor control).In this model, the dynamics of the field, the stator and damping windings are considered. The electrical equations are as follows [15]:

$$V_d = R_S i_d + \frac{d}{dt}\varphi_q - \omega_R \varphi_q \quad (1)$$

$$V_q = R_S i_q + \frac{d}{dt}\varphi_q + \omega_R \varphi_d \quad (2)$$

$$V_{fd}^{'} = R_{fd}^{'} i_{fd}^{'} + \frac{d}{dt}\varphi_{fd}^{'} \quad (3)$$

$$V_{kd}^{'} = R_{kd}^{'} i_{kd}^{'} + \frac{d}{dt}\varphi_{kd}^{'} \quad (4)$$

$$V_{kq1}^{'} = R_{kq1}^{'} i_{kq1}^{'} + \frac{d}{dt}\varphi_{kq1}^{'} \quad (5)$$

$$V_{kq2}^{'} = R_{kq2}^{'} i_{kq2}^{'} + \frac{d}{dt}\varphi_{kq2}^{'} \quad (6)$$

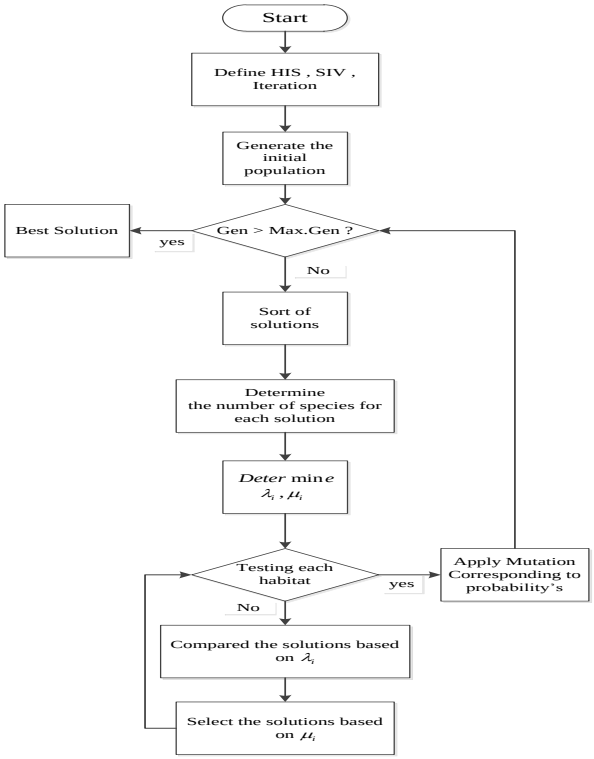

Fig. 2. The flowchart of Biogeography-Based Optimization Algorithm

Where, R_S , $R_{fd}^{'}$ and $R_k^{'}$ are stator and field and damper winding resistor, respectively. φ_d , $\varphi_f^{'}$ and $\varphi_k^{'}$ are stator and field and damper magnetic flux, respectively.

SSSC model

SSSC is one of the FACTS devices, which is connected in series with the power system. SSSC can generate inductive or capacitive voltage, which is independent from the line current. The injected voltage (V_q) is capable of changing the impedance of the transmission line from inductive to capacitive. SSSC injects the voltage V_q to the transmission line and the active and reactive power flow in transmission line are controlled by controlling the amplitude and the angle of V_q. The variation of V_q takes place via the voltage source converter, connected to the coupling transformer [7]. To feed the transformer and converter losses and to hold the capacitor charged, a small amount of active power is received from transmission line. In addition, in this paper the converter is used with IGBT switches, which are operated based on Pulse Width Modulation (PWM). The DC capacitor differential equation can be expressed as below [16]:

$$\frac{dV_{dc}}{dt} = \frac{3}{2C} km(I_D \cos\varphi + I_Q \sin\varphi) - \frac{V_{dc}}{CR_P} \quad (7)$$

Where, m and k are the modulation ratio and the ratio between the ac and dc voltage, C is the capacitor value, V_{dc} is the dc voltage, I_D and I_Q are the line current in D and Q axis, respectively.

4. Damping Controller

A. *The structures of PSS and SSSC Damping Controller*

The configuration of SSSC damping controller is displayed in Figure 3. The lead-lag controller is preferred by power system utilities, due to the ease in its on-line training and the lack of guaranteed stability by some adaptive and variable structure approaches. The input and output signals of the controller are $\Delta\omega$ and V_q.

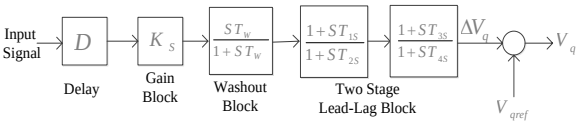

Fig. 3. The structure of SSSC Controller

The structure consists of a gain K_S, a washout signal block and a two-stage lead-lag block. The washout signal block, with a time constant T_W, is used as a high-pass filter. T_W is large enough to pass the input signal, including fluctuations, unchanged. The amount of T_W is not acute and can be in a range from 1 to 20 seconds. The lead-lag blocks (time

constants T_{1S}, T_{2S}, T_{3S} and T_{4S}) provide the appropriate specified phase-lead for the phase-lag offset between the input and the output. In figure 4, V_{qref} shows the reference injected voltage, which is obtained from the steady state power flow.

Fig. 4 demonstrates the configuration of the power system stabilizer (PSS) used in this paper. The structure includes a gain block K_{PS}, a washout signal block and a two-stage phase compensation block. The input and output signals of the PSS are $\Delta\omega$ and V_S, respectively. V_S is supplemented to the reference voltage of the excitation system.

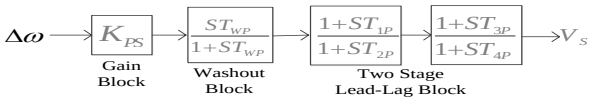

Fig. 4. The structure of Power System Stabilizer

Local input signals to control the FACTS devices include the active power, the line reactive power, the line current and the bus voltage magnitude. From these signals, the active power and line current are used as inputs in the papers. Similarly, remote signals are the speed deviation ($\Delta\omega$) and the generator rotor angle deviation ($\Delta\delta$).According to [17], the rotor speed deviation is an appropriate alternative as input signal for FACTS device controllers. Consequently, it is used as the input signal in this paper. Using the remote signals as the input signals means that the information is received with a time delay. Time delays make the system's performance degraded, therefore they must be considered in the design of the controller for the power system. However, the time delay is not considered in previous research work.

In this paper, for PSS, a sensor with time constant of 20 ms is considered and for SSSC damping controller a signal transmission time delay equal to 50 ms is considered, along 20 ms time constant of sensor.

Problem definition

In the lead-lag Controller structure, time constant T_W is normally a predetermined amount. $T_W = T_{WP} = 10s$ is used in this paper. The controller gains K_S, K_{PS} and time constants T_{1i}, T_{2i}, T_{3i} and T_{4i} are determined using the Biogeography-Based optimization algorithm. In steady state conditions, V_{qref} is constant value and ΔV_q is equal to zero. While in dynamic conditions, the injected series voltage, V_q, is adjusted so that to damp oscillations of the power system. The effective value of V_q is calculated as follows:

$$V_q = V_{qref} + \Delta V_q \tag{8}$$

Parameters of PSS and SSSC controller are designed so that after a large disturbance, to damp power system oscillations. These oscillations can be seen by changing in the rotor angle, rotor speed and etc. Since, most of the power systems operating conditions are varied; a performance index for a wide range of set points is defined as follows:

For single-machine power system:

$$J = \int_{t=0}^{t=t_1} |\Delta\omega|.t.dt \tag{9}$$

For two-machine power system:

$$J = \int_{t=0}^{t=t_1} |\omega_1 - \omega_2|.t.dt \tag{10}$$

Where, $\Delta\omega$ is the speed deviation in SMIB, ω_1 and ω_2 are the first and second generator speeds, respectively, and t_1 is the simulation time. To calculate the objective function, a time-domain simulation has been done and for improved power system oscillation damping and improved stability, minimization of the objective function is performed. Problem constraints are the range of PSS and SSSC damping controller parameters. As a result, the coordinated design of PSS and SSSC damping controller can be considered as an optimization problem as follows:

Minimize J

Subject to:

$$K_{i_{MIN}} \le K_i \le K_{i_{MAX}} \tag{11}$$

$$K_{i_{MIN}} \le K_i \le K_{i_{MAX}} \tag{12}$$

Typical ranges of the optimized parameters are [0.01–100] for K_i and [0.01–1] for T_{1i} ,T_{2i}, T_{3i} and T_{4i} [18]. The process of optimizing the objective function by Biogeography-Based Optimization algorithm and the time-domain simulation for setting the parameters is performed. In BBO, the search for the optimal parameters to achieve a unique solution is continued. Because of the strength of this algorithm, the parameters are set and the solution is not trapped in a local minimum. In this paper, for appropriate operation of BBO, number of habitats, keep rate and mutation are respectively: 50, 0.2 and 0.1. Also in PSO, swarm size, $\varphi 1 = \varphi 2$ and $C1 = C2$ respectively: 50, 2.05, 1.496 have been selected.

The designed controllers with the algorithms take place in different performance conditions of the

system, the desired performance conditions are considered as in Table 1.

Table.1.
The loading condition

Operating condition	P(pu)	Q(pu)	X_L(pu)
Nominal	0.8	0.114	0.3
Light	0.2	0.01	0.3
Heavy	1.2	0.4	0.3

The optimized parameters based on BBO and PSO algorithms are shown in Table 2 and Table 3.

Table.2.
Optimized parameters in smib

Power system	**SMIB**			
Algorithms	PSO		BBO	
The Parameters	PSS	SSSC	PSS	SSSC
K	54.12	78.45	41.21	62.35
T1	0. 9541	0.41	0.2154	0.1845
T2	0.2154	0.54	0.4547	0.8746
T3	0.3254	0.741	0.5586	0.8978
T4	0.5614	0.4124	0.7451	0.3821

Table.3.
Optimized parameters in multi-machine

Power system	**SMIB**			
Algorithms	PSO		Algorithms	
The Parameters	PSS	The Parameters	PSS	The Parameters
K	78.2	84.41	69.69	78.42
T1	0.234	0.41	0.19	0.71
T2	0.014	0.31	0.048	0.21
T3	0.024	0.74	0.45	0.019
T4	0.104	0.21	0.045	0.56

5. Simulation Results

The proposed coordinated controller for the SSSC and the PSS have been simulated in single-machine and two machine power systems under different disturbances and the results have been compared with each other. The simulation is done in MATLAB SimPowerSystems toolbox.

A. Single Machine Infinite Bus Power System

Single machine infinite bus system with SSSC is shown in Figure 5. The system includes a synchronous generator, the coupling transformer, SSSC and two parallel transmission lines. In this figure, T represents the transformer, V_T and V_B are the terminal voltage of the generator and the infinite bus voltage, respectively, V_1, V_2, V_3, V_{DC}, V_q and I are the bus voltages, DC link voltage, the injected voltage of SSSC and the line current, respectively.

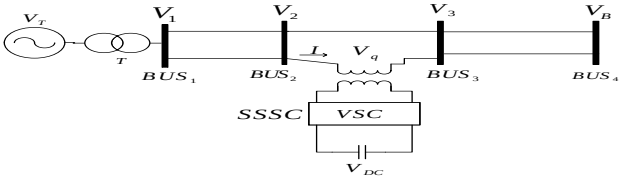

Single machine infinite-bus power system with SSSC

The coordinated controller is simulated in different operating conditions (light, Nominal, heavy) in a SMIB under different perturbation as follows.

1) 3-phase fault disturbance – Nominal loading condition

A three-phase to ground short circuit on the line between buses 3 and 4, close to the bus 3 in parallel transmission line with SSSC has happened and lasted for 100 ms. After clearing the fault, the system is restored to its initial state. The simulation results are shown in Figure 6. According to Figure 6, when SSSC damping controller is not used (Without any controller), the low frequency oscillations are not damped and the power system became unstable, while both coordinated controller damp the oscillations well and improve the dynamic stability. Compared with the PSO controller, it is clear that the BBO controller effectively increases the power system damping and stability by adjusting the injected voltage of SSSC.

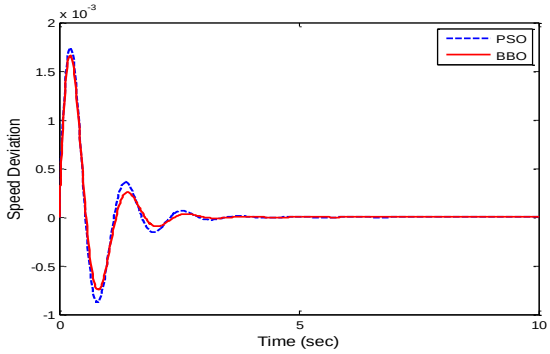

(a)

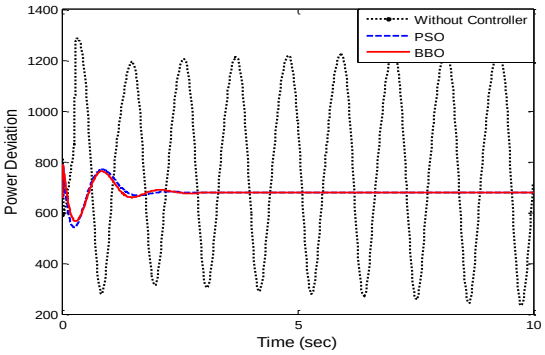

(b)

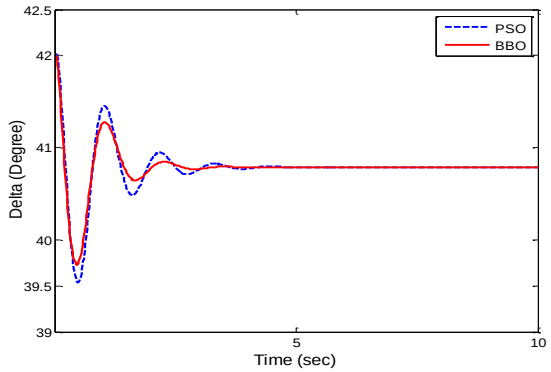

(c)

Fig. 5. System response for 3-phase fault: (a) Speed Deviation (b) Power Deviation (c) Power angle deviation

2) *2-phase fault disturbance – Heavy loading condition*

A two-phase to ground short circuit on the line between buses 1 and 2, close to the bus 2 in transmission line with SSSC has happened and lasted for 100 ms. Similar to the previous case, after clearing the fault, the system is restored to its initial state. The simulation results are shown in Figure 7. According to this figure, the BBO controller efficiently increases the power system damping by adjusting the injected voltage of SSSC compared to PSO controller.

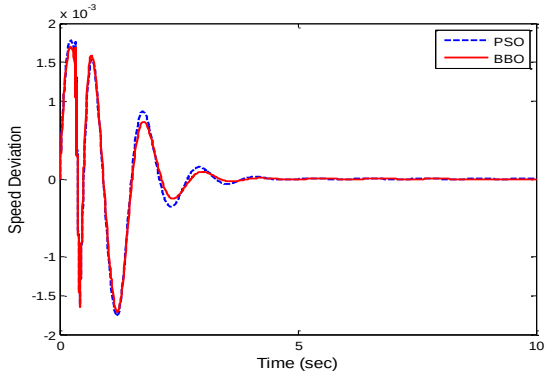

Fig. 6. Speed deviation for 2-phase fault – Heavy loading condition

3) *Single phase fault disturbance - Light loading condition*

A single-phase to ground short circuit on the line between buses 1 and 2, close to the bus 1 has happened and lasted for 100 ms. After clearing the fault, the system is restored to its initial state. Simulation results are shown in Figure 8. According to this figure, the BBO controller efficiently increases the power system damping by adjusting the injected voltage of SSSC. Here, the impact of the proposed coordinated controller, with changing in signal transmission in various conditions, is simulated and the results under different transmission delays are shown. It is clear that with the increase in time delay, the performance of the proposed controller deteriorates and with the decrease in transmission delay, the performance of the controller improves.

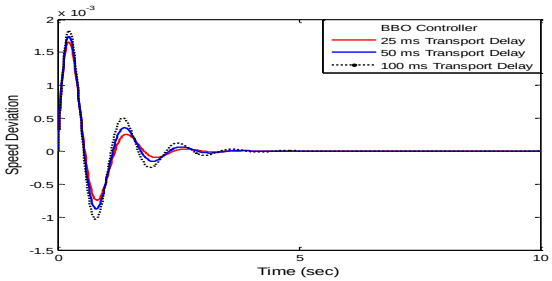

Fig. 7. Speed deviation for single-phase fault - for various signal transmission delays

4) *Two-machine power system*

Fig. 9 shows the single line diagram of the two-machine power system [19]. A SSSC is located between buses 3 and 4 on mid-point of the tie-line, to improve the stability of the power system. The speed difference between the first and the second generator ($\omega_1 - \omega_2$) is used as the input signal of the SSSC controller. The simulation results are obtained under the following conditions.

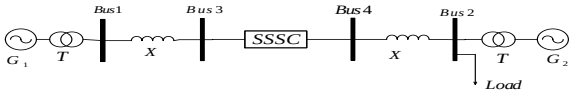

Fig. 8. Two-machine power system

5) *Single phase fault disturbance*

A single-phase to ground short circuit on the line between buses 1 and 3, close to the bus 1 has happened and lasted for 100 ms. After clearing the fault, the system is restored to its initial state. Simulation results are shown in Figure 10. According to this figure, both local and inter-area modes of oscillations in the absence of controllers are highly unstable while damping controller designed by intelligent algorithms efficiently increases the power system damping by adjusting the injected voltage of SSSC. Damping controller based on BBO damped the system oscillations faster than the PSO controller. Considering the efficiency of the proposed controller in the two-machine power system, it can be extended to larger power systems, too.

6) *Small disturbance*

A disconnecting load is simulated at bus 2 for 100 ms. Again after clearing the fault, the system is restored to its initial state. Simulation results are shown in Figure 11. This simulation is performed by BBO controller in different signal transmission delay. When SSSC damping controller is not used, the low frequency oscillations are not damped and

the power system becomes unstable while BBO controller efficiently increases the power system damping. In addition to, it is clear that with the decrease in signal transmission delay, the performance of the controller improves.

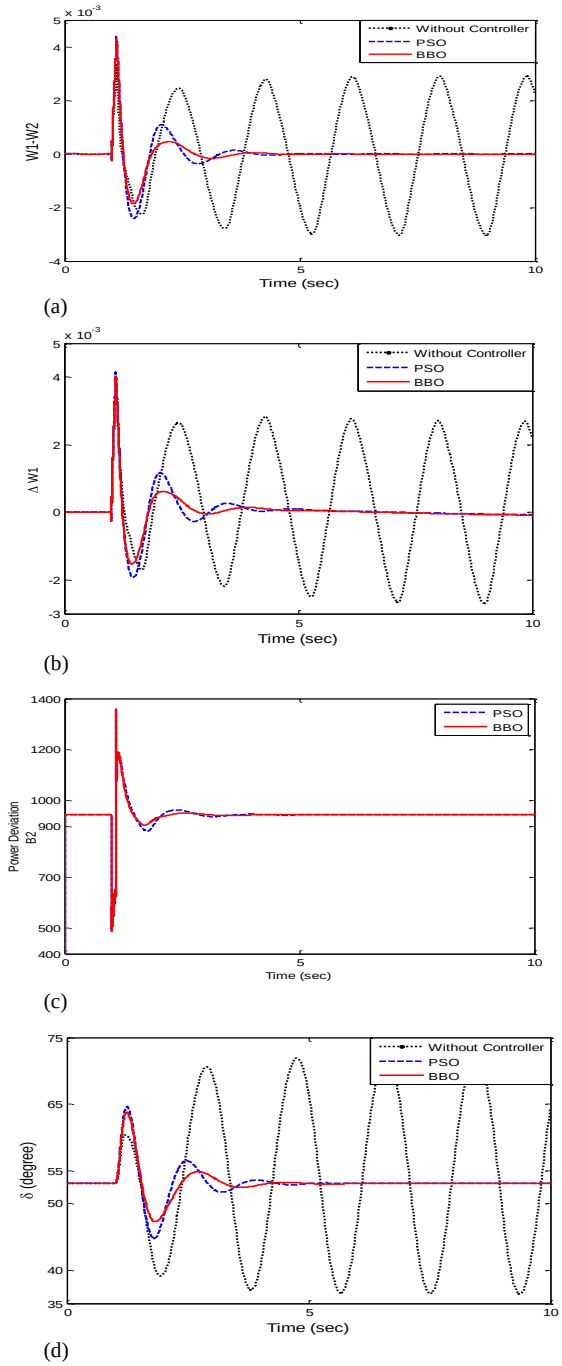

Fig. 9. System response for single-phase fault: (a) Inter-area mode of oscillation (b) Local mode of oscillation (c) Tie-line power flow (d) Power angle deviation

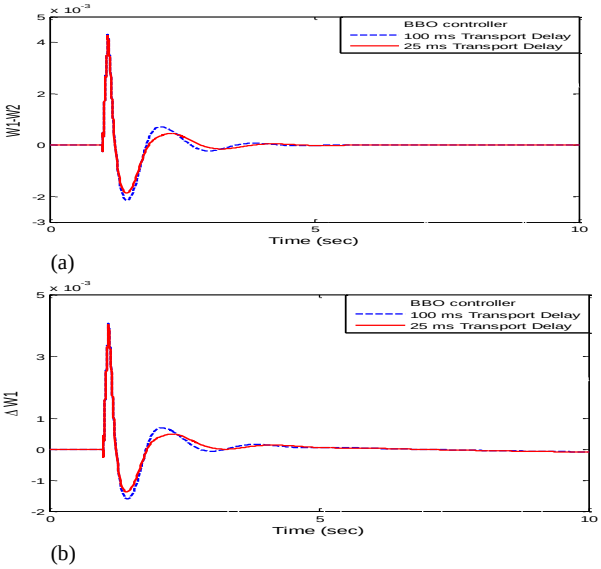

Fig. 10. System Response For Small Disturbance: (a) Inter-area mode of oscillation (b) Local mode of oscillation

6. CONCLUSION

In this paper, the application of the coordinated design damping controller is shown to improve the power system stability. To minimize fluctuations of the power system, time domain simulation of the proposed controller was accomplished. Biogeography-Based Optimization algorithm was used to adjust, coordinate and optimize the control parameters. The coordinated controller is simulated in single-machine and two machine power systems and the results were compared. The simulation results under different disturbances in both power systems indicate the effectiveness of the coordinated controller for SSSC. The controller has damped the local and inter-area oscillations well, and has improved the dynamic stability. The coordinated design of the damping controller based on BBO damped system oscillations faster than the PSO controller and the dynamic stability of the network is further improved. In addition to, with changing in signal transmission in various conditions, is specified that with the increase in time delay, the performance of the proposed controller deteriorates and with the decrease in transmission delay, the performance of the controller improves.

References

[1] Kundur, P. Power system stability and control, New York: McGraw-Hill, 1994.

[2] Tanaka, S. Power system stabilizer, Google Patents, 1990.

[3] Sinha, S. K., Patel R. N, and Prasad R. "Applications of FACTS devices with Fuzzy controller for oscillation damping in AGC," Recent Advancements in Electrical, Electronics and Control Engineering (ICONRAEeCE), IEEE, December, pp. 314-318, 2011.

[4] Chang, Y, and Xu Z. "A novel SVC supplementary controller based on wide area signals," Electric Power

Systems Research, Vol. 77, No. 12, pp. 1569-1574, 2007. DOI: 10.1109/PES.2006.

[5] Duangkamol, K, Mitani Y, Tsuji K, and Hojo M. "Fault current limiting and power system stabilization by static synchronous series compensator," Power System Technology, 2000. Proc. PowerCon 2000. IEEE, Vol. 3, pp. 1581-1586, 2000.

[6] Larsen, E.V, Sanchez-Gasca J.J, and Chow J.H. 1 "Concepts for Design of FACTS Controllers to Damp Power Swings," Power Systems, IEEE Transaction on, Vol. 10, No. 2, pp. 948-956.1995.

[7] Jowder, F. A. L. "Influence of mode of operation of the SSSC on the small disturbance and transient stability of a radial power system," Power Systems, IEEE Transactions on, Vol. 20, No. 2, pp. 935–942, 2005.

[8] Falehi, A.D, Rostami M, and Doroudi A. "Coordinated design of PSSs and SSSC-based damping controller based on GA optimization technique for damping of power system multi-mode oscillations," Power Electronics, Drive Systems and Technologies Conference (PEDSTC), 2nd, pp. 199–204, 2011.

[9] Ali, E. S, and Abd-Elazim S.M. "Hybrid BFOA-PSO approach for SSSC damping controller design," Control, Decision and Information Technologies (CoDIT), International Conference on, pp. 464-469, 2013.

[10] Shayeghi, H, Shayanfar H. A, Jalilzadeh, S, and Safari A. "Tuning of damping controller for UPFC using quantum particle swarm optimizer," Energy Conversion and Management, Vol. 51, pp. 2299-2306, 2010.

[11] Fernández-Comesana, P, Doval-Gandoy J, Diaz-Dorado E, and Alvira-Baeza D. "Evolutive algorithm to optimize the power flow in a network using series compensators," Compatibility and Power Electronics, CPE'09, pp. 43–47, 2009.

[12] Simon, D. "Biogeography-based optimization," Evolutionary Computation, IEEE Transactions on, Vol. 12, No. 6, pp. 702-713, 2008.

[13] Roy, P. K, and Mandal D. "Quasi-oppositional biogeography-based optimization for multi-objective optimal power flow," Electric Power Components and Systems, Vol. 40, No. 2, pp. 236-256, 2011.

[14] Bhattacharya, A, and Chattopadhyay PK. "Biogeography-based optimization for solution of optimal power flow problem," Electrical Engineering/Electronics Computer Telecommunications and Information Technology (ECTI-CON), pp. 435-439, 2010.

[15] Sauer, P, and Pai M. Power system dynamics and stability , New Jersey: Prentice Hall, 1998.

[16] Wang, H. F. "Static synchronous series compensator to damp power system oscillations," Electric Power Systems Research, Vol. 54, No. 2, pp. 113-119, 2000.

[17] Mohapatra, SK, and Panda S. "A Comparative Study Between Local and Remote Signal Using Shunt Facts Compensator Based Damping Controller," International Journal on Electrical Engineering and Informatics, Vol. 5, No. 2, pp. 135-153, June 2013.

[18] Shayeghi, H, Safari, A, and Shayanfar H. A. "PSS and TCSC damping controller coordinated design using PSO in multi-machine power system," Energy Conversion and Management, Vol. 51, No. 12, pp. 2930-2937, 2010.

[19] Anderson, PM, and Fouad AA. Power System Control and Stability , Ames, IA: Iowa State Univ. Press, first edition, 1977.

Neuro-Fuzzy Based Algorithm for Online Dynamic Voltage Stability Status Prediction Using Wide-Area Phasor Measurements

Ahmad Ahmadi[1] ,Yousef Alinezhad Beromi[2]

[1]Department of Electrical Engineering, Semnan University, Semnan, Iran.A.Ahmadi@students.semnan.ac.*ir*

Abstract

In this paper, a novel neuro-fuzzy based method combined with a feature selection technique is proposed for online dynamic voltage stability status prediction of power system. This technique uses synchronized phasors measured by phasor measurement units (PMUs) in a wide-area measurement system. In order to minimize the number of neuro-fuzzy inputs, training time and complication of neuro-fuzzy system, the Pearson feature selection technique is exploited to select set of input variables that have the strongest correlation with the output. Study on the network features such as phase angle and voltage amplitude has shown that among two interesting features, phase angle has maximum information about the performance of the network and solely can be used for training purposes. This is extra advantage of the proposed method that minimum data is needed to predict dynamic voltage stability status The efficiency of the proposed dynamic voltage stability prediction method is verified by simulation results of New England 39-bus and IEEE 68-bus test systems. Simulation results show that the proposed algorithm is accurate, computationally very fast and reliable. Moreover, it requires minimum data and so it is desirable for Wide Area Monitoring System (WAMS).

Keywords: Dynamic voltage stability prediction; Wide area monitoring system; Neuro-fuzzy algorithm; Feature selection technique

1. Introduction

Voltage stability is an important subset of power system stability factors which refers to the ability of a power system to maintain steady voltages at all buses in the system after being subjected to a disturbance caused by a given initial operating condition [1]. Voltage instability problems may occur for a variety of causes such as increased loading on transmission lines, on-load tap changer dynamics and reactive power constraints [2]. For convenience of analysis and gaining insight in to the nature of voltage stability problems, it is useful to characterize voltage stability in terms of Large-disturbance and Small-disturbance voltage stability [1]. Small disturbance voltage stability is the ability of a power system to maintain voltages for small disturbances such as changes in load or voltage at a bus; while, large-disturbance voltage stability refers to the ability of a power system to maintain voltages for large disturbances such as faults on the power system. Voltage stability can be analyzed using static or dynamic tools. Static analysis based on load flow methods, are widely used to determine the voltage stability margin indexes and to achieve fast approximate analysis of long-term voltage stability [3]. Despite the fact that static analysis provides suitable information about static voltage stability margin, it neglects all dynamic elements and considers that instability is caused by the active power or reactive power unbalance. On the other hand, voltage instability is

a dynamic phenomenon under large or small disturbance. The static analysis methods are not able to correctly evaluate small disturbance voltage stability problems. Study on dynamic voltage stability has been presented by different researchers [3-5]. From small signal point of view, voltage stability is achieved when damping ratio of critical mode is positive and as a result the system oscillations are damped. Otherwise, a pair of complex and critical eigenvalue of the system will place in the right half of complex plane and consequently, damping is negative which leads to undamped oscillations of power system [4]. Complexity and nonlinearity of power systems, especially on consumer side, online identifying and detecting operation point status of these systems has become more vital. Whereas, online information regarding power system status, provides an appropriate tools for power system operators to better implementation corrective and preventive strategies such as using compensators or changing load and generation arrangement to improve power system stability. Thus, together with load prediction which has attracted considerable attention, predicting operation status of power system is also important. As a result, in recent studies Neural network as a reliable and intelligent method has received widespread attention from researchers for dynamic stability prediction [3,6-8]. Another necessity in running online algorithm is availability of information about the whole network. In recent years, the presence of PMUs with modern communication facilities has been one of the most encounters in development of smart grids [9,10]. With this technology, it is possible for real time application to measure voltage magnitude and phase angle information more rapidly and precisely. In this paper a classification for operation status of power systems respect to dynamic voltage stability boundary is presented and relation between each operating point and mentioned classification is predicted by using a hybrid strategy include of PMU data, feature selection method and neuro-fuzzy system (NFS). The superiority of the NFS comparing to neural network is that neural networks work as black boxes and cannot use prior knowledge. NFS can utilize almost the same learning methods and achieve the same accuracy as neural network, yet the knowledge in the form of fuzzy rules is easily interpretable for humans [11,12]. Our proposed method has two advantages. First, the tuning algorithms for our proposed method are back propagation learning and least mean square estimation [13,14] which are fast and robust. These algorithms are employed by ANFIS toolbox in Matlab Software. Second, a feature selection algorithm is employed in addition to using NFS. This will decrease number of input features to the NFS leading to a faster response of NFS. The feature selection algorithm used in this paper is based on [15]. Choosing an effective set of input data is important since we need maximum information about the system while minimum numbers of inputs are employed. To have such an advantage, [16] proposed using voltage magnitude and phase angle to train the neural network. It was mentioned that this features are suitable enough to get good training and prediction for a network. In this paper it is demonstrated that even using phase angle, the system stability is reasonably predictable. Furthermore, the number of phase angles can be decreased using a feature selection algorithm. As a result optimum prediction with minimum input data is obtained. Contributions of the paper can be summarized as follows:

Regardless of literatures which voltage stability margin of power system is evaluated, in this paper, voltage stability problem is analyzed and predicted in the form of a classification problem in which NFS algorithm is used as a predictor.

Owing to nonlinear behavior of Eigenvalues of dynamic algebraic Jacobian of power system, analyzing and obtaining HB boundary is more complicated comparing to SNB boundary. Thus, in this paper a solution for investigating power system status based on this boundary without solving dynamic algebraic equations of power system is suggested.

Here, it is shown that the phase angles obtained from PMUs are enough for training when NFS is employed; whereas, voltage amplitude and phase angle were presented as the best training data in [16].

Phase angles in buses that provide redundant data are omitted imposing feature selection algorithm that results in fewer numbers of features used for training.

The remaining parts of the paper are organized as follows. The dynamic voltage stability boundary is presented in section II. The proposed prediction strategy composed of feature selection technique and NFS, based on PMU data is presented in section III. Obtained simulation results for New England 39 bus and IEEE 68 bus test systems are presented and discussed in section IV. Finally, conclusion is made in section V.

2. The dynamic voltage stability boundary

Unlike the static voltage stability analysis methods, the dynamic voltage stability assessment methods, which usually use the time-domain simulation results, accurately model the power system components to detect both short-term and long-term voltage instabilities [5]. The dynamic

voltage stability methods investigate the conditions of the system around equilibrium point which means that the system has nonlinear dynamic and performance. To calculate dynamic stability of the system in each equilibrium point on P-V curve, following equation is used. Equation (1) defines nature of the system in each instant which is in the form of parameter dependent differential-algebraic equations [4],

$$\begin{aligned} \dot{x} &= f(x,y,p) \qquad f: R^{n+m+k} \to R^{n} \\ g(x,y,p) &= 0 \qquad g: R^{n+m+k} \to R^{m} \end{aligned} \tag{1}$$

where

$x \in X \subseteq R^{n}$, $y \in Y \subseteq R^{m}$, and $p \in P \subseteq R^{k}$. P serves as system operation conditions, including loads, generation, etc. Generation dynamics of power systems are represented by dynamic state variables, x. As an example exciter control systems may be mentioned. Algebraic criterions, such as power flow equations, are fulfilled by instantaneous variables, y. considering constant values for p parameters, an equilibrium point is a solution of the system:

$$\dot{x} = 0 \Rightarrow f(x,y,p) = 0 \quad \text{subject to constraints } g(x,y,p) = 0 \tag{2}$$

To evaluate performance of the system and its response to small disturbances, the linearized model of the system at the equilibrium point is calculated. Linearization can be utilized to determine stability margin of the equilibrium point. So one may rewrite the above model as:

$$\begin{bmatrix} \Delta\dot{x} \\ 0 \end{bmatrix} = \begin{bmatrix} \frac{\partial f}{\partial x} & \frac{\partial f}{\partial y} \\ \frac{\partial g}{\partial x} & \frac{\partial g}{\partial y} \end{bmatrix} = \begin{bmatrix} J_{11} & J_{12} \\ J_{21} & J_{22} \end{bmatrix} \begin{bmatrix} \Delta x \\ \Delta y \end{bmatrix} = J \begin{bmatrix} \Delta x \\ \Delta y \end{bmatrix}, \tag{3}$$

$$p \in Const, \quad \frac{\partial f}{\partial p} = 0, \quad \frac{\partial g}{\partial p} = 0$$

where J is called the unreduced Jacobian, augmented Jacobian, or augmented system state matrix [4]. Parameter p was assumed to have small and slow variations. Equation (3) can be reduced to ordinary state space equations by eliminating Δy :

$$\Delta\dot{x} = (J_{11} - J_{12}J_{22}^{-1}J_{12})\Delta x = A\Delta x \tag{4}$$

where A is called reduced Jacobian or reduced system matrix. In power system studies, dynamic-algebric Jacobian matrix is used in order to obtain accurate dynamic voltage stability boundaries [4,17]. For a structural stability problem, there are three different kinds of bifurcation points which they are Hopf bifurcation (HB), Saddle-node bifurcation (SNB) and Singularity induced bifurcation (SIB). In this paper, Hopf bifurcation boundary is used for determining the dynamic voltage stability status of the system in response to a small disturbance. The distance between the base load and the load level leading to the occurrence of HB, is called the voltage stability dynamic loading limit. The problems related to oscillations in the power system are associated with the lack of damping in critical modes [18]. Consider a complex eigenvalue of β±α- =ζ. In such circumstances, the damping ratio of such a mode is defined as follows: In the above equation, α and β are the real and imaginary parts of the critical eigenvalues of the reduced dynamic algebraic Jacobian of the power system. In addition, according to the above relation, Hopf bifurcation occurs when the critical eigenvalues damping ratio of the system is zero and this mode corresponds to the situation, where the eigenvalue is placed on the imaginary axis of the complex plane. Moreover, this mode corresponds to undamped oscillations of the power system's parameters, such as voltage or generated reactive power of generators. On the other hand, based on the dynamic algebraic Jacobian of the power system, voltage stability holds when all the eigenvalues are on the left side of the imaginary axis, so in this situation, the damping is positive and system oscillations are damped. Additionally, in the loadings more than the load leading to HB, the damping ratio (σ) is negative, which is in parallel with undamped oscillations. In "Fig. 1" the behavior of the system's critical eigenvalues is shown at different load levels (λ). In this figure, the oscillatory behavior of the power system is shown, which corresponds to the behavior of critical eigenvalues.

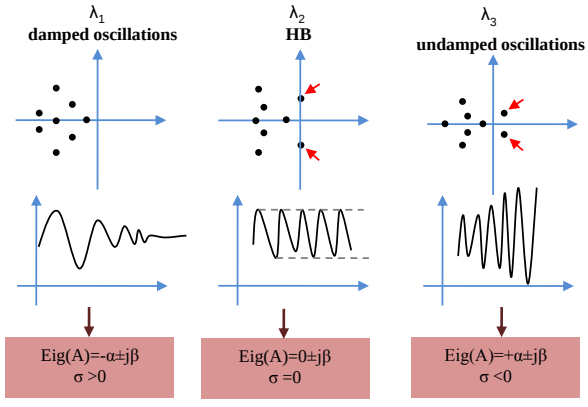

Fig. 1. Relation between the critical eigenvalues of dynamic algebraic Jacobian and power system oscillations

3. Proposed method for dynamic voltage stability status prediction

The proposed prediction method for timely and accurate dynamic voltage stability status prediction consists of synchrophasors recorded by WAMS, feature selection technique and Neuro-Fuzzy classifier as the forecast engine. The flowchart of the proposed algorithm is shown in "Fig.2". In this figure, is a vector containing voltage magnitudes and phase angles of all buses which are obtained

from PMUs. Additionally, is the set of selected inputs for dynamic voltage stability status forecast process which are obtained using the proposed feature selection technique. Finally, NFS is employed to predict the dynamic voltage stability status of the system. The other parts of the flowchart are explained in following sections.

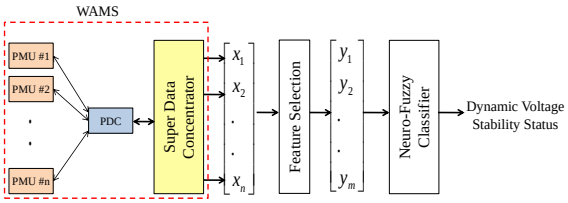

Fig. 2. Proposed algorithm for dynamic voltage stability status prediction

A) Wide-area measurement system

WAMS contains PMUs, communication links, phasor data concentrators (PDCs) and super data concentrator and/or control centers. PMUs can provide synchronous measurement with high sampling rate e.g. 30 samples per second, that results in time based tracking of phenomena in the network [9,19]. Therefore, conventional methods have been replaced with WAMS based on PMUs. The PMUs are mounted on different buses and provide magnitude and phase angle of voltages and currents. They also measure frequency and rate of frequency variation. In this paper, we use this superior advantage of PMUs to study dynamic voltage stability of the network and to develop our proposed method.

B) Feature selection algorithm

Candidate set of input for a practical power system are not applicable to a forecaster since they may be so large. Moreover, due to presence of irrelevant and redundant inputs the forecast engine might be misled. Redundant data increases the computation time in processor, does not provide more information. The method used in this paper in order to optimize the data set is Pearson future selection algorithm [15]. To introduce the algorithm, assume that we have feature set with values and the classes Y with values y- where in our case X could be any combination of the vector variables (V, δ) and Y is the vector of classified data (0,1)- then Pearson's linear correlation coefficient is computed exploiting following equation:

$$\rho(X,Y)=\frac{E(XY)-E(X)E(Y)}{\sqrt{\sigma^2(X)\sigma^2(Y)}} \quad (5)$$

The probability of variables correlation is gained using error function as follows:

$$P(X\sim Y)=erf\left(|\rho(X,Y)|\sqrt{n/2}\right) \quad (6)$$

where n is number of samples. Then, the features are sorted based on value of $P(X\sim Y)$ and the one with maximum rank ($P(X\sim Y)$) has the first place in the list. Depending on the design process, the k (chosen by designer based on complication of the design and number of features which are needed. features with maximum rank could be chosen to train the neuro-fuzzy system. The performance of the feature selection is illustrated in "Fig.3". The general case was depicted where two variables (V, δ) are included in measured data. As the figure shows, correlation of each feature with output is ranked and then the most top ranks are chosen to train neuro-fuzzy system.

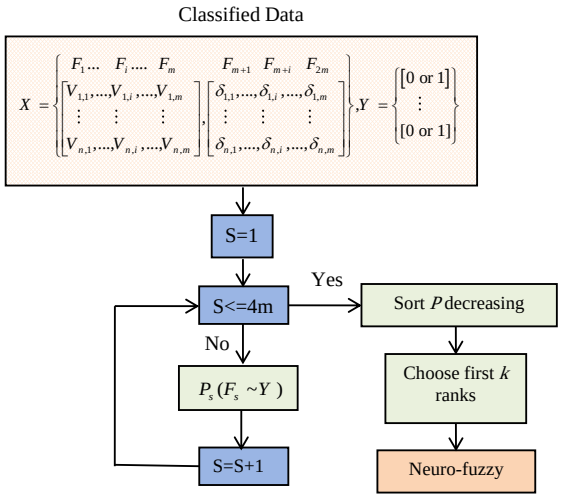

Pearson feature selection algorithm

C) Neuro-fuzzy predictor

In this paper we employ neuro-fuzzy inference system to predict the stability of the network. The general model of the neuro-fuzzy system is depicted in "Fig. 4". The method used for neuro-fuzzy system is based on Takagi and Sugeno's method [11,12]. Takagi Sugeno's method was chosen because it can be tuned more flexibly to estimate performance of nonlinear systems. For the involved system with m inputs, fuzzy if-then rules can be presented as:

$$\begin{aligned}&\text{Rule1: if } x_1 \text{ is } A_{1,1} \text{ and .... } x_n \text{ is } A_{1,n},\\ &\text{then } y_1 = w_{1,1}x_1 + w_{1,2}x_2 + ..., w_{1,n}x_n + r_1\\ &\text{Rule2: if } x_1 \text{ is } A_{2,1} \text{ and .... } x_n \text{ is } A_{2,n},\\ &\text{then } y_2 = w_{2,1}x_1 + w_{2,2}x_2 + ..., w_{2,n}x_n + r_2\end{aligned} \quad (7)$$

$w_{k,i}$ is parameter tuned by the neuro-fuzzy system, $k=1,...,N$ is number of rules, and $i=1,...,n$ is number of inputs of neuro-fuzzy

systems. y_k is output of each rule in Takagi Sugeno's type fuzzy systems. The output of each rule is linear combination of inputs plus a constant. This format is useful when training algorithm is used to tune coefficients.

In "Fig. 4", we have five layers that are briefly described as follows. Layer 1 is responsible for the fuzzification of input variables and converts the input variables to linguistic variables. Therefore, each circle in layer 1 is a membership function related to its inputs. If we suppose that we have n inputs and for each input we have m membership function (equal membership function is defined for simplicity in notation, while it can be different in real application), therefore the membership function equation can be written as follows:

$$f_{i,j} = \mu_{i,j}(x_i) \quad (8)$$

where $j = 1,...,m$ is number of membership functions in the i[th] fuzzy set and $f_{i,j}$ is the firing strength of input i in membership function, $\mu_{i,j}$ .In our case, bell-shaped membership function is used.

$$\mu_{i,j}(x_i) = \exp(-(\frac{x_i - a_{i,j}}{b_{i,j}})^2) \quad (9)$$

Variations of $a_{i,j}$ and $b_{i,j}$ produce different membership functions. Here, the back propagation algorithm [13,14] is implemented to tune parameters of membership functions.

In layer 2, the product is used which is denoted by Π. Layer 2 computes the firing strength of each rule. As the figure shows, we have different connections from layer 1 to layer 2 that describe the varieties of rules. Suppose that inputs of the first node in layer 2 are $\mu_{1,1}, \mu_{2,1}, ..., \mu_{n,1}$, then the output of layer 2 is computed by the following product function:

$$R_k = \mu_{1,1}(x_1) \times \mu_{2,1}(x_2) \times .... \times \mu_{n,1}(x_n) \quad (10)$$

Layer 3 normalizes the output of each rule and prepares them for second part of the neuro-fuzzy system for training purpose. Therefore the output of the k^{th} circle in layer 3 is:

$$NR_k = \frac{R_k}{R_1 + R_2 + ... + R_N} \quad (11)$$

where NR_k stands for normalized rules. These values are final value of each rule in fuzzy system. Then, it is exerted to second part of neuro-fuzzy system. From "Fig. 4" we see that we have the same number of nodes as layer 3. For each node we have one input that comes from the previous layer and m inputs that are the original inputs of neuro-fuzzy systems. The output of k^{th} node in layer 4 is:

$$O_k = NR_k(w_{k,1}x_1 + w_{k,2}x_2 + ... + w_{k,n}x_n + r_k) \quad (12)$$

To tune parameters $w_{k,i}$, least mean square error algorithm is used [13,14]. The most important feature of least mean square algorithm is that it always provides global minima. Therefore, the best approximated parameters can be obtained. The final layer, layer 5, is a single node that is summation of all incoming signals,

$$Y = \sum_{k=1}^{N} O_k \quad (13)$$

In our case, desired output is a discrete function $\{0,1\}$ while the output of the neuro-fuzzy system is continuous function. In training phase, desired outputs are exerted to the neuro-fuzzy system, however, when the training phase is finished, we add a threshold to the end of neuro-fuzzy system to provide discrete response.

$$Y_{decision} = \begin{cases} 0 & Y < 0.5 \\ 1 & Y \geq 0.5 \end{cases} \quad (14)$$

Actually, this does not change performance of the neuro-fuzzy system and just discretizes the response so that it can be clearly understandable that system is stable or unstable based on the classification performed in the next sections. In this paper, different input variables are considered and for each one a neuro-fuzzy system is trained and results are analyzed. The measured and classified data are divided to two groups; training data and testing data. This separation is performed so that we have enough data for training and some data for testing the trained system. The separation is performed randomly through all data. The detailed description is given in the simulation part.

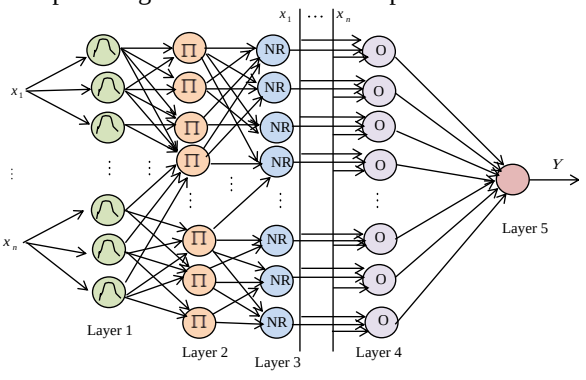

Fig. 3. The structure of neuro-fuzzy system

4. Development of the proposed modeling and simulation results

The proposed dynamic voltage stability prediction method is applied to New England which has 39 buses, 10 machines and 46 branches and IEEE 68 bus test system which has 68 buses, 16

machines and 83 branches. These test systems are used frequently for voltage stability studies of power system [4]. Dynamic and static data of these test systems can be found in [20,21]. The set of candidate inputs for New-England and IEEE 68 bus test systems are 39V+39δ =78 and 68V+68δ =136 candidates, respectively. Moreover, for each proposed class label, 300 samples are generated from which 260 and 40 samples are devoted to training and test phases, respectively. The whole steps to implement neuro-fuzzy predictor are depicted in "Fig. 5". According to mentioned proposed algorithm, it has been assumed that PMUs are installed at buses in the network to measure the voltage synchrophasors. In this paper, these synchrophasors which are used for training the NFS were generated through offline time domain simulations using DIgSILENT software [22]. To produce samples, the small disturbance voltage stability was considered which includes changes in the system load (both the load level and load distribution). Dynamic voltage stability status for each sample is determined using modal analysis [10] with following condition function,

$$\begin{cases} EP\ is\ befor\ HP \Rightarrow & \text{system is stable, class: 1} \\ EP\ is\ after\ HP \Rightarrow & \text{system is unstable, class: 0} \end{cases} \quad (15)$$

where EP is equilibrium point and HP is Hopf Bifurcation boundary.

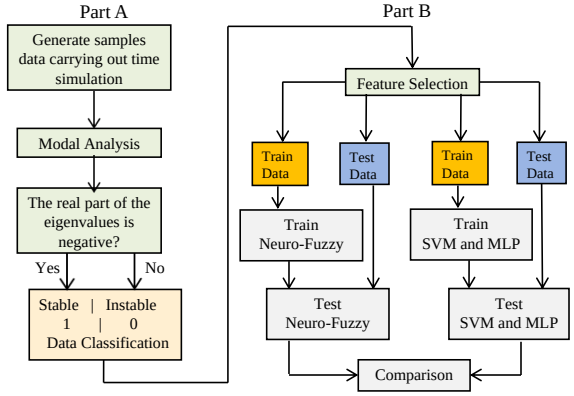

Fig. 4. Dynamic Simulation of system and training procedure

After performing modal analysis, samples are classified under two groups, stable or unstable. Then, the feature selection algorithm is exerted to this classified data to select the most informative features and Finally the selected features is exerted to three different forecast engines include of NFS, support vector machine (SVM) [23] and multi layer perception (MLP) [23] based back propagation (BP) learning algorithms for training purpose. , MLP and SVM neural networks are used as alternative of NFS forecast engine.

A) Simulation results for New England test system

Experiment.1. Selection of Input features

At first, we test neuro-fuzzy system with whole voltage magnitudes and phase angles data and then we show that the voltage magnitudes can be omitted and using just phase angles is enough for suitable training of NFS. In this experiment, Prediction errors obtained by proposed feature selection method for three different forecast engines are shown in "table 1".

These results clearly demonstrate that NFS operates more precisely than other forecast engines specially MLP regarding prediction of operating condition based on proposed classification. Prediction error might cause the operator to fail in making correct decision and to apply a wrong corrective/preventive method which, in turn, may cause damage to the system. For example if the forecast engine predicts class 1 instead of class 2 (a condition when damping is negative and critical eigenvalue is in the right half of complex plane), system damping would be desirable from operator's perspective and it would not be necessary to increase damping. It may result in severe fluctuations and moves the system to vicinity of collapse. Moreover, it can be observed from "Table 1" that we can achieve suitable prediction using only phase angle features. To analyze this issue more properly, the voltage magnitudes and phase angels of some buses are demonstrated in "Fig. 6" when small disturbances (simultaneous increase in loads of buses number 15, 16 and 18) occur.

Table.1.
Obtained prediction error for NFS, SVM and MLP – New-England (Experiment. 1)

Input feature sets	voltage magnitudes and phase angles (V ,δ)	phase angles (δ)
No. of features	40	10
No. of rules	40	8
No. of clustering	22	8
Prediction error of NFS(%)	0	0
Prediction error of SVM (%)	3.75	2.5
Prediction error of MLP_{BP} (%)	5	3.75

From "Fig. 6", it can be observed that the variations of the voltage magnitude from stability point to instability point are too small. Here, we have phase angles which have much faster and larger variations comparing to voltage magnitudes. Moreover, it can be concluded from simulation results that the phase angle can provide enough information about stability of the system. Considering these two facts, we suggested to ignoring all the voltage magnitude features from our data. In "Table 2" The phase angle features

were chosen using proposed feature selection algorithm are shown and the rank of each candidate is sorted according to their information value for the forecast process.

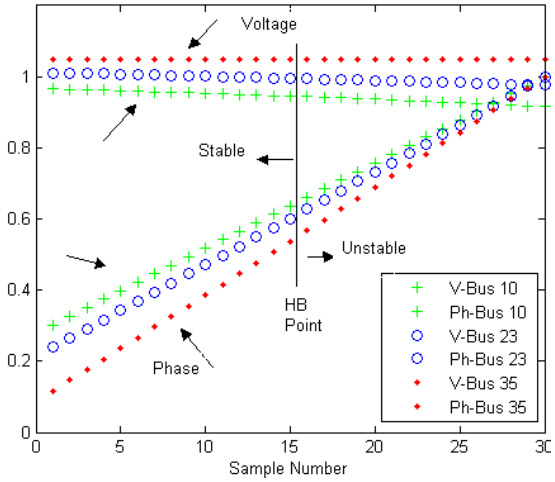

Fig. 5. The sample data from voltage magnitudes and phase angles of some buses during small disturbance

Table.2.
The selected phase angle features after employing feature selection for New England test system

Selected features	δ_{26}	δ_{27}	δ_{25}	δ_{11}	δ_{28}
Rank	0.551	0.543	0.524	0.520	0.519
Selected features	δ_{7}	δ_{30}	δ_{29}	δ_{13}	δ_{8}
Rank	0.513	0.509	0.509	0.500	0.495

Experiment.2. PMU Measurement Error

Despite precision of PMUs, signal processing may produce some errors in the phasor calculations. Difference between the exact applied signal and the measured one is defined as total vector error (TVE). According to IEEE standard [24], the TVE must be less than 1% under steady state condition. To assess performance of the proposed prediction strategy, the effect of noisy samples is evaluated in this experiment. To this purpose, a random error between 0 and 1% was added to voltage phasor of all buses achieved by DIGSILENT before using them as inputs to the NFS, SVM and MLP forecast engines.

"Table 3" shows the results obtained from this experiment. As shown in this table, 14 of 39 initial candidate features are selected after performing the proposed feature selection method. While in the first experiment 10 of 39 initial candidate features are selected. This difference indicates that the complex quality samples lead to increase in the amount of input features of forecast engine. This increase is inevitable in order to increase the accuracy or decrease the error of forecast engine. However, the presented prediction error in "Table 3" shows that the proposed forecast engine (NFS) have zero prediction error while SVM and MLP_{BP} have 5% (4 of 80 test samples are predicted incorrectly) and 7.5 (6 of 80 test samples are predicted incorrectly) prediction error, respectively.

Table.3.
Obtained prediction error for NFS, SVM and MLP considering measurement error– New-England test system (Experiment. 2)

Input feature sets	phase angles
No. of features	14
No. of rules	14
No. of clustering	11
Prediction error of NFS(%)	0
Prediction error of SVM (%)	5
Prediction error of MLP_{BP} (%)	7.5

B) Simulation results for IEEE 68-bus test system

To investigate the capabilities of proposed prediction method, two experiments performed in previous section are carried out on the IEEE 68 bus test system as well. "Table 4", shows prediction results of NFS, SVM and MLP forecast engines for two mentioned experiments. The noise applied in experiment 2 is the same as what applied in experiment 2 of New-England test system. The selected phase angle features for experiment-1 after employing feature selection and rank of each candidate is sorted in "Table 5".

Table.4.
Obtained prediction error for NFS, SVM and MLP – IEEE 68-bus test system

	Experiment-1		**Experiment-2**
Input feature sets	(V, δ)	(δ)	(δ)
No. of features	50	20	34
No. of rules	45	16	30
No. of clustering	30	12	22
Prediction error of NFS(%)	0	0	1.25
Prediction error of SVM (%)	3.75	2.5	6.25
Prediction error of MLP_{BP} (%)	6.25	3.75	8.75

Table.5.
The selected phase angle features after employing feature selection for IEEE 68-Bus test system

Selected features	δ_{55}	δ_{15}	δ_{54}	δ_{16}	δ_{14}
Rank	0.6927	0.6926	0.6926	0.6925	0.6904
Selected features	δ_{17}	δ_{8}	δ_{63}	δ_{36}	δ_{64}
Rank	0.6621	0.6576	0.6552	0.6551	0.6524
Selected features	δ_{37}	δ_{9}	δ_{35}	δ_{20}	δ_{43}
Rank	0.6523	0.6512	0.6503	0.6489	0.6479
Selected features	δ_{19}	δ_{22}	δ_{21}	δ_{58}	δ_{52}
Rank	0.6471	0.6469	0.6469	0.6467	0.6456

According to "Table 4" in experiments 1 and 2 NFS have less prediction error in contrast with

SVM and MLP. As a result using NFS with feature selection algorithm is powerful method to predict dynamic voltage stability status of the power system. Also according to the results, using the phase angle features alone is sufficient to predict the voltage stability status. Hence, using the proposed method, the status of power system voltage stability via minimum number of features can be predicted with good accuracy.

5. Conclusion

In this paper, neuro-fuzzy predictor was designed to estimate the dynamic voltage stability status of the system based on wide area synchrophasor data. In order to reduce the number of neuro-fuzzy inputs, training time and complication of forecast engine, the feature selection technique combined with neuro-fuzzy system is proposed to select the set of input variables that have the strongest correlation with the output. The proposed method has been implemented on New-England and IEEE 68-bus test systems. The capabilities of proposed NFS are compared to other neural networks including SVM and MLP for two input feature sets considering noisy input data. The obtained numerical results revealed that proposed prediction method properly specify power system voltage stability status with a few number of phase angle features.

References

[1] Kundur P, Paserba J, Ajjarapu V, Anderson G, Bose A, Canizares CA. "Definition and classification of power system stability," *IEEE Transactions on Power Systems*, Vol. 19, No. 2, pp. 1387–1401, 2004.

[2] Taylor, C.W. "Power system voltage stability," *McGraw-Hill*, 1994.

[3] NimaAmjady, Mohammad HosseinVelayati. "Dynamic voltage stability prediction of power systems by a new feature selection technique and probabilistic neural network," Euro. Trans. Electr. Power, Vol. 21, No. 1, pp. 312–328, 2011.

[4] Amjadi, N, Ansari, M. R. "Small disturbance voltage stability assessment of power systems by modal analysis and dynamic simulation," International Journal of Energy Conversion and Management, Vol. 49, No. 10, pp. 2629-2641, 2008.

[5] H. Khoshkhoo, S. M. Shahrtash. "On line dynamic voltage instability prediction based on decision tree supported by a wide area measurement system," *IET Gener. Transm.Distrib*, Vol. 6, No. 11, pp. 1143-1152, 2012.

[6] A.R. Bahmanyar, A. Karami. "Power system voltage stability monitoring using artificial neural networks with a reduced set of inputs," Int. J. of Electrical Power & Energy Systems, Vol. 58, pp. 246-256, 2014.

[7] Kamalasadan, S., Thukaram, D., Srivastava, A. K. "A New Intelligent Algorithm for Online Voltage Stability Assessment and Monitoring," Int. J. of Electrical Power & Energy Systems, Vol. 31, No. 2-3 ,pp. 100-110, 2009.

[8] Chakrabarti, S. "Voltage Stability Monitoring by Artificial Neural Network Using a Regression-based Feature Selection Method," Expert Systems with Applications, Vol. 35, No. 4, pp. 1802-1808, 2008.

[9] Fahd Hashiesh, Hossam E. Mostafa, Abdel-RahmanKhatib, Ibrahim Helal, and Mohamed M. Mansour. "An Intelligent Wide Area Synchrophasor Based System for Predicting and Mitigating Transient Instabilities," IEEE Trans. Smart Grid, Vol. 3, No. 2, pp. 645-652, 2012.

[10] F. Li,W. Qiao, H. Sun, H. Wan, J.Wang, Y. Xia, Z. Zhu, and P. Zhang. "smart transmission grid, Visionand framework," IEEE Trans. Smart Grid, Vol. 1, No. 2, pp. 168-177, 2010.

[11] Y. Zhou, A. Dexter. "Off-line identification of nonlinear, dynamic systems using neuro-fuzzy modeling technique," Fuzzy Sets and Systems, Vol. 225, pp. 74-92, 2013.

[12] C. J. Lin, C. H. Chen. "Identification and prediction using recurrent compensatory neuro-fuzzy systems," Fuzzy Sets and Systems, Vol. 150, No. 2, pp. 307-330, 2005.

[13] A. Abraham. "Neuro fuzzy systems, state-of-art modeling techniques," Artifial Intelligence, Springer-Verlag Germany, Jose Mira, 2001.

[14] J. S. R. Jang. "ANFIS, adaptive-network-based fuzzy inference system," IEEE Trans On Systems, Man and Cybernetics, Vol. 23, No. 3, pp. 665-685, 2002.

[15] J. Biesiada, W. Duch. "Feature selection for high-dimensional data: a pearson redundancy based filter," Division of Computer Methods, Dept. of Electro technology, The Silesian University of Technology, pp. 242-249, 2007.

[16] Q. Zhou, U. D. Annakkage, A. D. Rajapakse. "Online monitoring of voltage stability margin using and artificial neural network," IEEE Trans. On Power Syst, Vol. 25, No. 3, pp. 1566-1574, 2010.

[17] Huang GM, Zhao L, Song X. "A new bifurcation analysis for power system dynamic voltage stability studies," In: Proc IEEE power eng.soc winter meeting, Vol.2, No. , pp. 882–887, 2002.

[18] Mithulananthan, N., Canizares, C. "Effect of Static Load Models on Hopf Bifurcation Point and Critical Modes of Power Systems," Thammasat Int. J. SC. Tech, Vol. 9, No. 4, pp. 69-76, 2004.

[19] A. G. Phadke and J. S. Thorp. "synchronized phasor measurements and their applications," New York, NY, USA, Springer 2008.

[20] Pai MA, Energy function analysis for power system stability', Boston/USA:Kluwer 1989.

[21] http://www.ee.washington.edu/research/pstca/.

[22] DIgSILENT user manual toolbox. Available at: http://www.digsilent.de/

[23] MATLAB neural network toolbox, the mathworks, available: http://www.mathworks.com/.

[24] IEEE Standard for Synchrophasors for Power Systems, IEEE Std. C37. 118-2005, pp. 1–57, 2005.